Short title: Screening for *ibm2* suppressors identified FPA

Corresponding author:
Nicolas BOUCHÉ
Tel: +33 1 30 83 31 71
E-mail: Nicolas.Bouche@inra.fr

Antagonistic actions of FPA and IBM2 regulate transcript processing from genes containing heterochromatin

Aurélie Deremetz[1,2], Clémentine Le Roux[3], Yassir Idir[1,2], Cécile Brousse[1], Astrid Agorio[1], Isabelle Gy[1], Jane E. Parker[3] and Nicolas Bouché[1]

Affiliations:
[1] Institut Jean-Pierre Bourgin, UMR1318, INRA, 78000 Versailles, France
[2] Université Paris-Sud, Université Paris-Saclay, 91405 Orsay, France
[3] Max-Planck Institute for Plant Breeding Research, Department of Plant-Microbe Interactions, D-50829 Cologne, Germany

Summary sentence:
Intronic heterochromatic marks, associated with alternative polyadenylation sites, are decoded by RNA-binding proteins like FPA and IBM2, to tune the expression of key regulator genes such as *IBM1* or *RPP7*.

Author contributions:
AD, CLR, YI, CB, AA, IG and NB performed the research; AD, CLR, YI and NB analyzed the data; NB designed the research; JP and NB wrote the paper.

ABSTRACT

Repressive epigenetic marks, such as DNA and histone methylation, are sometimes located within introns. In Arabidopsis (*Arabidopsis thaliana*), INCREASE IN BONSAI METHYLATION2 (IBM2), an RNA-binding protein containing a BAH domain, is required to process functional transcript isoforms of genes carrying intronic heterochromatin. In a genetic screen for suppressors of the *ibm2* mutation, we identified FPA, an RNA-binding protein which promotes use of proximal polyadenylation sites in genes targeted by IBM2, including *IBM1* encoding an essential H3K9 histone demethylase and the disease resistance gene *RECOGNITION OF PERONOSPORA PARASITICA7* (*RPP7*). Both IBM2 and FPA are involved in the processing of their common mRNA targets: transcription of IBM2 target genes is restored when *FPA* is mutated in *ibm2* and impaired in transgenic plants over-expressing *FPA*. By contrast, transposons targeted by IBM2 and localised outside introns are not under this antagonistic control. The DNA methylation patterns of some genes and transposons are modified in *fpa* plants, including the large intron of *IBM1*, but these changes are rather limited and reversed when the mutant is complemented, indicating that FPA has a restricted role in mediating silencing. These data reveal a complex regulation by IBM2 and FPA pathways in processing mRNAs of genes bearing heterochromatic marks.

Keywords

Arabidopsis;

FPA;

INCREASE IN BONSAI METHYLATION (IBM1 & IBM2);

mRNA processing;

RECOGNITION OF PERONOSPORA PARASITICA7 (RPP7).

INTRODUCTION

DNA and histone methylations are epigenetic marks found in plants and animals that influence chromatin structure and have a direct impact on gene function and transposon mobilization. Chromatin can be modified and remodeled in several ways. In plants, the Jumonji C (JmjC) domain-containing protein INCREASE IN BONSAI METHYLATION1 (IBM1) is a histone demethylase which removes methylation on lysine 9 of histone H3 (H3K9me). IBM1 function is essential in plants because it prevents deposition of these heterochromatic silencing marks at transcribed genes (Saze et al., 2008; Miura et al., 2009; Inagaki et al., 2010). H3K9me and CHG DNA methylation (where H = A, T or C) are tightly correlated. Indeed, CHG methylation is controlled by the DNA methyltransferase CHROMOMETHYLASE3 (CMT3) recruited to regions enriched in H3K9me, which it directly binds (Du et al., 2012; Du et al., 2014). In a reciprocal manner, H3K9me is catalysed by three histone methyltransferases, SU(VAR)3-9 HOMOLOG4 / KRYPTONITE (SUVH4/KYP), SUVH5, and SUVH6 (Ebbs and Bender, 2006). KYP binds CHG-methylated cytosines through its SRA domain (Johnson et al., 2007). Thus, CMT3 and KYP participate in a self-reinforcing loop between DNA and histone methylation, which is needed for silencing transposons and repeat sequences but is deleterious to genes when IBM1 is absent. Consequently, *ibm1* mutants accumulate both H3K9me and CHG in coding regions with drastic consequences for development (Saze et al., 2008; Miura et al., 2009).

Two other categories of Arabidopsis (*Arabidopsis thaliana*) mutants share the *ibm1* developmental and molecular phenotype: mutants of the *IBM2 / ANTI-SILENCING1 / SHOOT GROWTH1* gene, hereafter called *IBM2* (Saze et al., 2013; Wang et al., 2013; Coustham et al., 2014) and mutants of *ENHANCED DOWNY MILDEW2* (*EDM2*) (Tsuchiya and Eulgem, 2013). The *IBM1* gene encodes two different transcripts of which only the longest encodes a functional protein (Rigal et al., 2012), and its production is controlled by both IBM2 and EDM2 in a yet unclear manner. IBM2 is a protein of unknown function containing a Bromo-Adjacent Homology (BAH) domain and an RNA-Recognition Motif (RRM) (Saze et al., 2013; Wang et al., 2013; Coustham et al., 2014). EDM2 contains several zinc-finger domains and a region similar to the active domains of certain methyltransferases (Tsuchiya and Eulgem, 2013). Both EDM2 and IBM2 are found in the same protein complex, bridged by the ASI1-IMMUNOPRECIPITATED PROTEIN1 (AIPP1) (Duan et al., 2017). In addition to the *IBM1* gene, EDM2, AIPP1 and IBM2 share another target, the disease resistance gene *RECOGNITION OF PERONOSPORA PARASITICA7* (*RPP7*) (Saze et al., 2013; Tsuchiya and

Eulgem, 2013; Wang et al., 2013; Lai et al., 2018). Like *IBM1*, *RPP7* contains a heterochromatic domain within a long (>2 kb) intron associated with H3K9me and DNA methylated in all cytosine contexts. The IBM2 complex associates with these methylated intronic regions (Saze et al., 2013; Tsuchiya and Eulgem, 2013; Wang et al., 2013) to produce the full-length functional transcript by an unknown molecular mechanism. One hypothesis is that EDM2/AIPP1/IBM2 function by enhancing the use of distal polyadenylation sites over proximal sites located in large introns.

Polyadenylation is one key mRNA processing step, and the choice between alternative polyadenylation sites impacts the regulation of gene expression. FPA is an RNA-binding protein with three RRMs involved in polyadenylation site choice and plays a major role in repressing floral transition by favoring the proximal polyadenylation site of an antisense of the *FLOWERING LOCUS C* (*FLC*) transcript (Hornyik et al., 2010; Liu et al., 2010) and more broadly in regulating the 3′-end site choice of diverse mRNAs (Sonmez et al., 2011; Duc et al., 2013), including its own transcript (Macknight et al., 2002; Hornyik et al., 2010). So far, FPA has not been identified as a member of any splicing or polyadenylation complexes, and the precise function of FPA and its mode of action are still unclear. *fpa* mutants have also been identified in a genetic screen aimed at finding components required for RNA-mediated chromatin silencing (Bäurle et al., 2007), but the role played by FPA in silencing has not been explored. In addition, FPA is involved in plant defense responses (Lyons et al., 2013), pointing toward a more general role in addition to flowering.

Here, we identify *fpa* as a suppressor of the *ibm2* phenotype. The transcription of both *IBM1* and *RPP7* is restored in a double *fpa ibm2* mutant and impaired when *FPA* is over-expressed. We show that *fpa* mutants are depleted in CHG methylated cytosine within the largest introns of *IBM1*, providing evidence that mutating *FPA* has an effect on chromatin structure that nevertheless seems to be limited to specific regions. We demonstrate that RNA-binding proteins, like FPA and IBM2, are involved in an intricate crosstalk between chromatin and RNA processing to regulate the production of key genes such as *IBM1* and *RPP7*. We further show that transposons controlled by IBM2 localised outside introns are unaffected by this mechanism.

RESULTS

fpa is a genetic suppressor of *ibm2*

To uncover new genes impacting the function of *IBM2*, we performed a forward genetic screen to isolate suppressors of *ibm2-4,* an allele previously called *sg1-1* (Coustham et al., 2014). Approximately 7,000 *ibm2-4* seeds were treated with EMS (see Materials & Methods). The genetic screen was performed in two steps on 88,000 M3 seedlings. Because the *ibm2* phenotype is related to a deficiency in production of the long functional *IBM1* mRNA (Saze et al., 2013; Wang et al., 2013; Coustham et al., 2014), we screened for mutants showing a wild-type phenotype, aiming to select suppressors in which the function of *IBM1* was restored. We postulated that this pool of plants contained suppressors of *ibm2*, but also suppressors restoring the effects of a non-functional IBM1. Mutations like *cmt3* or *kyp,* for instance, suppress *ibm1* by preventing the accumulation of heterochromatic marks on a large range of IBM1 targets (Saze et al., 2008). These mutations did not restore the transcription of IBM2 targets such as *AT3G05410* or *RPP7* (Supplemental Figure S1). Next, to isolate genetic suppressors of *ibm2* more specifically from the first screen, we determined the level of transcription of *AT3G05410* (Saze et al., 2013; Wang et al., 2013), a target of IBM2 which is not targeted by IBM1. We isolated three M3 plants (from the same M2 pool) which resembled wild-type plants but had more serrated leaves (Figure 1A) and were late flowering (Supplemental Figure S2). In these plants, mRNA levels of the known IBM2 target *AT3G05410* were intermediate between *ibm2-4* and wild type (Supplemental Figure S3). Therefore, the three mutants are likely progeny from the same M2 plant. By sequencing and comparing the genomes of these plants and the original *ibm2-4* mutant, we identified mutations that were homozygous and common to the three plants but not the original mutant. Sequencing revealed that the suppressor of *ibm2-4* carries a nucleotide change (C-to-T) in the fifth exon of *FPA* (*AT2G43410*) at position 586, creating a premature stop codon. The *ibm2-4* suppressor was therefore designated a new *fpa* allele (*fpa-11*). These results show that *fpa* is epistatic over *ibm2*.

We then extracted genomic DNA from leaves of *fpa-11 ibm2-4* mutants to perform whole-genome bisulfite single-base resolution sequencing (WGBS; Supplemental Table S1) and determine the patterns of methylation for genes. On average, both CG and CHH methylation levels were similar in genes of *ibm2-4* and *fpa-11 ibm2-4* mutants (Supplemental Figure S4), however, the CHG hypermethylation accumulating in *ibm2* genes (Saze et al., 2013; Wang et al., 2013; Coustham et al., 2014) was lost in genes of *fpa-11 ibm2-4* (Figure 1B). We confirmed the results by identifying the Differentially-Methylated Regions (DMRs) in *ibm2-4* or *fpa-11 ibm2-4* compared to wild type (Figure 1C). Indeed, the number of *ibm2* CHG hyperDMRs (n=4722) was reduced by 35-fold in *fpa-11 ibm2-4*, implying that mutating *FPA* in *ibm2* suppresses the CHG hypermethylation in genes.

Next, we quantified mRNA levels of known IBM2 targets (Supplemental Figure S5) in *fpa* and *fpa ibm2* mutants grown *in vitro* for 21 days. RT-qPCR analyses revealed that the *IBM1-L* transcripts were more abundant compared to wild type in all *fpa* allelic backgrounds tested, including *fpa-3*, which is a previously described allele (Hornyik et al., 2010), *fpa-11*, *fpa-3 ibm2-4*, and *fpa-11 ibm2-4* (Figure 2; *IBM1-L*). The opposite trend was observed for *IBM1-S* (Figure 2; *IBM1-S*). We also detected a general increase of *IBM1* transcripts in *fpa* mutants using a set of primers amplifying all *IBM1* transcript isoforms (Figure 2; *IBM1-total*). Together, the expression data show that mutating *FPA* in both *ibm2* and wild-type plants increased *IBM1* transcripts by ~1.8-fold. Furthermore, in *fpa* backgrounds, the production of the long *IBM1* transcript is favored over the shortest one. Levels of two other IBM2 targets (*AT3G05410* and *AT1G11270*) were restored to 40 % of wild type in the double *fpa ibm2* mutants (Figure 2; *AT3G05410-L* and *AT1G11270-L*). Finally, *RPP7* (*AT1G58602*) mRNA levels were restored to 80% of wild type in the suppressor *fpa ibm2* backgrounds (Figure 2; *RPP7-L*). Altogether, the genetic screen for *ibm2* suppressors, the methylome sequencing of *fpa ibm2* mutants, and the RT-qPCR analyses of IBM2 targets demonstrate that a mutation in *fpa* counterbalances the absence of IBM2 by restoring the production of its target transcripts.

FPA contributes to processing of IBM2 target genes containing intronic heterochromatin

To understand better the links between FPA and the processing of IBM2 targets, the levels of their transcripts were monitored when *FPA* was over-expressed. Compared to wild type, the production of *IBM1-L*, *RPP7-L*, *AT1G11270-L*, and *AT3G05410-L* mRNAs was reduced by 29%, 60%, 47%, and 54%, respectively, in plants expressing *35S*:*FPA-YFP* constructs in a *fpa-8* background (Figure 3 and Supplemental Figure S6). Therefore, the long *RPP7*, *IBM1*, *AT1G11270*, and *AT3G05410* transcripts are produced incorrectly in these transgenic plants, confirming the role played by FPA in their processing.

Next, we assessed the function of the Col-0 *RPP7* gene in race-specific disease resistance against the biotrophic oomycete *Hyaloperonospora parasitica* isolate Hiks1 (*Hpa* Hiks1) (Slusarenko and Schlaich, 2003). The triple *suvh456* mutant, which has lost the *RPP7* intragenic methylation, and two *ibm2* alleles (*ibm2-1* and *ibm2-4*) displayed reduced *RPP7* resistance, indicated by increased growth of *Hpa* Hiks1 in leaves (Figure 4), whereas *fpa-3* and *fpa-11* mutants were as resistant as Col-0 (Figure 4). In agreement with the partial restoration of *RPP7-L* transcript levels in *fpa-11 ibm2-4* (Figure 2), this double mutant also exhibited partially restored *RPP7*-mediated resistance (Figure 4). Therefore, FPA controls the resistance function of *RPP7*.

Direct RNA sequencing (DRS) helps to define polyadenylation sites by direct sequencing of RNAs in the absence of reverse transcription and is therefore a method of choice to localise regions where FPA promotes polyadenylation. We used the DRS data published previously for *fpa* mutants to identify polyadenylated 3' ends in *fpa-7* and Col-0 (Duc et al., 2013). We found that distant polyadenylation sites of *AT3G05410*, *IBM1*, and *RPP7* were more frequently used in *fpa* mutants at the expense of proximal polyadenylation sites (Figure 5). Indeed, the number of normalized DRS reads corresponding to distal polyadenylated sites increased in the *fpa-7* background by 2.4, 1.9, and 1.7 fold for *IBM1*, *AT3G05410*, and *RPP7*, respectively. By contrast, the number of DRS reads corresponding to proximal sites decreased by 28.8 and 3.4 fold for *IBM1* and *AT3G05410*, respectively. Hence, polyadenylation of IBM2 targets is mediated by FPA. The data indicate that FPA and IBM2 pathways are interconnected in processing of their common targets, including *IBM1* and *RPP7* transcripts.

IBM2 promotes the transcription of the methylated *Copia* element *AT4G16870* (Duan et al., 2017), which is a non-intronic transposon localized upstream of the *RPP4* resistant gene (Figure 6A). A chimeric *RPP4-AT4G16870* mRNA consisting of both *RPP4* and this *Copia* element (Wang and Warren, 2010) was detected in the wild type but not in *ibm2-4*, *aipp1-1*, *edm2-4*, or *suvh456* (Figure 6B and Supplemental Figure S7A), confirming that the transcription of *RPP4-AT4G16870* is promoted by an EDM2/AIPP1/IBM2 complex and relies on the presence of heterochromatic marks controlled by SUVH proteins. Similarly, *RPP4-AT4G16870* mRNAs were not detected in *fpa-11 ibm2-4* mutants but were expressed in *fpa-11* (Figure 6B). Thus, the loss of FPA does not restore the transcription of *RPP4-AT4G16870* mRNAs in *ibm2*. We verified that the *RPP4*-mediated resistance to *Hpa* isolate EMWA1 was not compromised in *ibm2, edm2, fpa ibm2,* or *fpa* mutants (Supplemental Figure S8). To identify additional non-intronic IBM2 targets, transposons differently expressed in *ibm2*, *edm2* and *aipp1*, compared to wild-type plants, were listed using published RNA-seq data (Duan et al., 2017). We found a total of 18 transposons that were significantly (FDR threshold ≤ 0.05) downregulated (log2FC(*ibm2* and *edm2* and *aipp1*/WT) < -2) in *ibm2*, *edm2*, and *aipp1* (Supplemental Table S2). Six transposons corresponded to known IBM2 targets like the intronic *RPP7* transposons or the *Copia* element *AT4G16870*. In addition, we found that *AT4TE21110* is another non-intronic IBM2 target expressed in Col-0 and *fpa* mutants but not in *ibm2* or *fpa ibm2* mutants (Figure 6C and Supplemental Figure S7B), as observed for *RPP4-AT4G16870*. Altogether, our data show that FPA and IBM2 pathways are antagonistic at genes containing heterochromatin within their introns, like *IBM1* or *RPP7,* but not at non-intronic IBM2 targets such as the *Copia* element *AT4G16870* or *AT4TE21110*.

Intronic DNA methylation of *IBM1* decreases in *fpa*

The genes targeted by IBM2 contain introns carrying heterochromatic marks which regulate their transcription. Since FPA was previously identified in a mutant screen for genes required for the silencing of an inverted repeat (Bäurle et al., 2007), we tested whether the DNA methylation patterns of IBM2 targets were modified in an *fpa* background. For this, we monitored methylation levels of the large *IBM1* intron in the *fpa* mutants. After bisulfite conversion, we sequenced the corresponding *IBM1* region in *ibm2-4*, *fpa-11 ibm2-4*, and *fpa-3*. Compared to wild type or to *ibm2* controls, CHG methylation was reduced by almost half in the *fpa-11 ibm2-4* and the *fpa-3* mutants (Figure 7A and Supplemental Figure S9). We examined the methylation patterns of the same *IBM1* region in mutants for which the whole methylomes were sequenced (Stroud et al., 2013), and we found reduced CHG methylation in both *fpa-7* and *fca-9 fpa-7* plants (Supplemental Figure S10). Therefore, the methylation of *IBM1* is modified in *fpa* backgrounds.

To explain the reduction of CHG methylation observed at *IBM1* in *fpa*, we hypothesized that IBM1 could control the production of its own mRNA by removing intronic epigenetic marks contained within the largest intron of the *IBM1* gene. If this hypothesis was correct, increased levels of *IBM1-L* transcript – as observed in *fpa* – would result in the demethylation of the *IBM1* intron. To test whether such a feedback loop exists, we monitored patterns of DNA methylation in the intron of *IBM1* when *IBM1-L* was over-expressed ectopically (Supplemental Figure S6). Indeed, IBM1 controls methylation of H3K9 which cross-regulates the levels of mCHG (Johnson et al., 2007; Du et al., 2012; Du et al., 2014). Our data show that cytosine methylation levels of the *IBM1* intron were comparable between wild type and *ibm1* mutants that over-express the *IBM1-L* cDNA (Figure 7A and Supplemental Figure S9). As the methylation patterns of the *IBM1* intron remained unchanged when *IBM1-L* was more abundant, we concluded that the hypomethylation of *IBM1* in *fpa* is likely not associated with the increased production of *IBM1-L* transcripts observed in this mutant background.

The absence of FPA induces transient methylation changes

To understand whether the decrease of methylation we observed for *IBM1* was widespread or limited to specific regions of the genome, we sequenced the whole methylome of *fpa* mutants. Levels of methylation per cytosine confirmed that biological replicates were closely correlated (Pairwise Pearson correlation values between biological replicates 0.97 for CGs, 0.98 for CHG and 0.94 for CHH). When the average methylation levels were calculated

in 100-bp windows partitioning the genome, we observed no broad changes between wild-type plants and *fpa-3* (Figure 8A), confirming results obtained with the *fpa*-7 T-DNA allele (Stroud et al., 2013). Next, we identified the DMRs in *fpa-3* and compared them to the wild type and to the transgenic *fpa-8* line complemented by a *35S:FPA-YFP* construct (Bäurle et al., 2007) that was also sequenced. The spontaneous DMRs naturally occurring within the Arabidopsis Col-0 accession were filtered (Zhang et al., 2018). We identified 61 CG hypoDMRs, 73 CG hyperDMRs, 7 CHG hypoDMRs, 7 CHG hyperDMRs, 2 CHH hypoDMRs, and 6 CHH hyperDMRs arising in *fpa-3* and returning to wild-type methylation patterns when the function of FPA was restored (Supplemental Table S3). Most of the CG hyperDMRs were found in genes (Figure 8B) and were *de novo* methylated in *fpa* (Figure 8C; *CGhyper*), while CG hypoDMRs overlapped with transposons (Figure 8B) that were demethylated in *fpa* (Figure 8C; *CGhypo*). The *IBM1* intronic region carrying the heterochromatic marks (Figure 7B) was identified among the 7 CHG hypoDMRs, confirming the results obtained by targeted bisulfite sequencing (Figure 7A and Supplemental Figure S9). A limited number of other regions remained differentially methylated in both *fpa-3* and the *fpa* complemented line compared to their respective wild-type controls: 12 CG hypoDMRs, 9 CG hyperDMRs, 2 CHG hypoDMRs, 2 CHG hyperDMRs and 1 CHH hypoDMR. Therefore, most of the changes of methylation patterns in *fpa*, including those at *IBM1*, are reversible when the mutant is complemented by a construct overexpressing *FPA*.

Next, we examined the methylation profiles of transposable elements that are derepressed in *fpa*. Previous studies have revealed that transposons like *AtSN1*, which is a SINE retroelement, *AtMu1*, which is a DNA transposon, and the helitron *AT1TE93275* are expressed in the *fpa* backgrounds in contrast to wild type (Bäurle et al., 2007; Sonmez et al., 2011). No changes in DNA methylation were observed for *AtMu1* in *fpa-3* or for *AtSN1* (Supplemental Figure S11). We confirmed that *AT1TE93275* is demethylated in all cytosine contexts in *fpa-3* (Supplemental Figure S11), matching one of the 4 CHG DMRs that remained hypomethylated when *fpa* was complemented. These results indicate that some transposons, which are up-regulated in *fpa*, are associated with differences in DNA methylation patterns, but their number is low because we found no widespread changes of transposon methylation patterns in *fpa*.

DISCUSSION

Here we identify *fpa* as a genetic suppressor of the *ibm2* mutation. The IBM2 protein complex interacts with heterochromatic marks localized within the large introns of IBM2 target

genes to promote production of their long transcripts. FPA, by promoting polyadenylation of shorter transcripts, antagonizes the function of IBM2. In addition, FPA affects methylation of the largest intron of *IBM1* and a limited number of other regions.

Crosstalk between FPA and IBM2 in polyadenylation site choice

Our forward genetic screen to isolate suppressors of *ibm2-4* revealed that FPA is involved in the processing of IBM2 targets. Levels of *AT1G11270* and *AT3G05410* long transcripts were restored to 40% of wild-type levels in a double *fpa-11 ibm2-4* mutant, and levels of *RPP7* long mRNAs were restored to 80% (Figure 2; *RPP7-L*). In addition, *IBM1* long mRNAs were ~1.8-fold more abundant in *fpa* compared to wild type (Figure 2; *IBM1-L*). Consequently, we found that the most distant polyadenylation sites of IBM2 target genes are favored in an *fpa* background (Figure 5). At the same time, the large intron of *IBM1* contained less methylation in *fpa* mutants (Figure 7, Supplemental Figure S9 and Table S3), although both CHG and H3K9 methylation within introns appear to be crucial for processing IBM2 target transcripts. First, these transcripts are incorrectly processed when intronic transposons are depleted of CHG methylation (Le et al., 2015). Indeed, RT-qPCR analyses revealed that levels of long *RPP7* and *AT3G05410* transcripts are reduced in *cmt3* (Le et al., 2015), confirming results obtained for *IBM1* long transcripts (Rigal et al., 2012). Second, compromising the functions of H3K9 histone methyltransferases has similar consequences. Northern blot analyses show that *kyp/suvh4* mutants produce lower levels of *IBM1* long transcripts compared to wild type (Rigal et al., 2012). If methylation marks are necessary to correctly transcribe IBM2 target genes, how then can IBM2 targets be transcribed in an *fpa* background in which intragenic heterochromatic marks are reduced? Because *fpa* is epistatic to *ibm2*, it is likely that IBM2 is important for the production of its target transcripts only when FPA is functional. A possible explanation is that FPA promotes the recruitment of the polyadenylation complex at proximal sites, while IBM2 antagonizes this binding. We suggest that IBM2 prevents the polyadenylation of short transcripts only when FPA is active. Whether IBM2 and/or its partners interact directly with proteins of the polyadenylation complex remains to be determined. This mechanism might apply to other plant species. In oil palm (*Elaeis guineensis*), for instance, the transcription of an essential homeotic gene is regulated by methylation of an intronic LINE retroelement (Ong-Abdullah et al., 2015). Levels of transcription also correlate with the size of heterochromatic regions. Expression of genes with long methylated introns, such as *RPP7*, *AT3G05410*, or *AT1G11270*, is decreased by more than 70% in *ibm2* and partially rescued in *fpa ibm2* (Figure 2). However, the transcription of *IBM1*, which contains a shorter methylated intronic region, is

decreased by only 50% in *ibm2* and restored in *fpa ibm2* (Figure 2) in which IBM1 is fully functional (Figure 1B and 1C). By inserting into introns, transposons introduce alternative polyadenylation sites, making the targeted gene regulated by both the IBM2 and FPA pathways. By contrast, FPA does not antagonize IBM2 for IBM2 transposon targets localized outside genic regions (Figure 6).

Links between RNA processing and methylation changes

The role played by FPA in controlling silencing remains controversial. The *fpa* mutants were first retrieved from a forward genetic screen to identify genes involved in RNA silencing (Bäurle et al., 2007). Even if some transposons are strongly reactivated in *fpa* (Bäurle et al., 2007; Sonmez et al., 2011), the analysis of DRS data showed no widespread differences of expression for transposons between *fpa-7* and the wild type (Duc et al., 2013). In addition, *fpa-7* methylome analyses revealed no major differences in methylation patterns (Stroud et al., 2013). *fpa-7* is a T-DNA allele, and recent studies have demonstrated that *fpa* mutations can rescue T-DNA insert mutants (Zhang et al., 2016), possibly explaining the phenotypic discrepancies existing between T-DNA and point mutation *fpa* alleles (Duc et al., 2013). By sequencing the methylome of the point mutation *fpa-3* allele, we confirmed that no major changes of DNA methylation patterns were observed genome-wide (Figure 8A), but we found that CG methylation was gained in some genes and lost in some transposons of *fpa* (Figure 8B and 8C). Most of these changes revert to wild-type patterns when the function of FPA is restored, indicating that the changes of methylation are rather limited and transient.

Mutating *FPA* more specifically disturbs DNA methylation of heterochromatic regions localised within the largest intron of *IBM1* in contrast to other IBM2 targets. By sequencing the methylome of *fpa-3*, the largest intron of *IBM1* was identified as a CHG hypomethylated DMR (out of 7 in total) (Supplemental Table S3), confirming results obtained by targeted bisulfite sequencing in *fpa-11 ibm2-4* (Figure 7A). Likewise, the CHG methylation, localized at the endogenous phytoene desaturase (*PDS*) locus silenced by an inverse repeat introduced transgenically *in trans*, is compromised in the *fpa-8* background (Bäurle et al., 2007). Hypomethylation of *IBM1* observed in *fpa* is probably not coupled to an increase of *IBM1-L* production, since transgenic *ibm1* plants overexpressing *IBM1-L* ectopically show no alteration of methylation at *IBM1* (Figure 7A and Supplemental Figure S9). Moreover, the limited number of CHG DMRs found in an *fpa* background (Supplemental Table S3) argue against FPA directly controlling the activity of CMTs at transposons localized near or within genes. Therefore, the loss of methylation at *IBM1* in *fpa* is probably independent of IBM1 activity. Other factors

might account for this hypomethylation, such as those associated with the changes of polyadenylation site in *fpa* mutants and the subsequent effects on *IBM1* mRNA processing. Previous studies have demonstrated that transcription initiation and/or the Pol II elongation rates are influenced by choice of polyadenylation sites at *FLC* (Wu et al., 2016). Similarly, Pol II occupancy is increased near the proximal polyadenylation sites of *RPP7* in *edm2*, *aipp1* and *suvh456* plants, indicating that the enzyme is probably pausing in this region (Lai et al., 2018). Therefore, changes of polyadenylation sites in *fpa* also very likely modify the rates of transcription for many genes, including *IBM1* and transposons, which might impact their methylation patterns. Furthermore, the recent discovery that human RBM15 proteins, related to FPA, direct methylation to specific non-coding RNAs (Patil et al., 2016), is consistent with a role for FPA in mRNA methylation, implying that a previously unrecognized interplay exists between epigenetic silencing marks and methylation of IBM2 target RNAs.

Conclusion

We show that FPA and IBM2 pathways are crucial for controlling the transcription of their common targets and provide evidence that they act antagonistically when transposons are inserted in introns. The tight regulatory control of *RPP7* mRNA levels is likely critical to limit the accumulation of a long functional *RPP7* transcript in pathogen-unchallenged conditions and to prevent autoimmunity. In the presence of *Hpa* Hiks1, the fine regulation of *RPP7* transcripts mediated by both IBM2 and FPA favors accumulation of a long transcript to induce a rapid and specific immune response (Tsuchiya and Eulgem, 2013). Similarly, the importance of H3K9 methylation in resistance to viruses has been described (Sun et al., 2015), and the virulence of geminiviruses requires a viral protein that inhibits expression of the main plant H3K9 methyltransferase, *KYP*. To reinforce the action of KYP, rapid modulation of *IBM1* gene expression, mediated by both FPA and IBM2, is likely essential. Our data suggest that intronic heterochromatic marks associated with alternative polyadenylation sites can be decoded by RNA-binding proteins like FPA and IBM2 to tune the expression of key regulator genes such as *IBM1* or *RPP7*.

MATERIALS AND METHODS

Plant materials and growth conditions

Arabidopsis (*Arabidopsis thaliana*) accession Ksk-1 was described previously (Slusarenko and Schlaich, 2003). All other plants were in the Arabidopsis Col-0 background.

The *ibm2-4* point mutation was previously named *sg1-1*, and *ibm2-5* (SAIL_310B06) was *sg1-2* (Coustham et al., 2014). The following mutants were previously described: *edm2-4* SALK_142563 (Eulgem et al., 2007), *fpa-3* (Hornyik et al., 2010), *fpa-7* (Michaels and Amasino, 2001; Veley and Michaels, 2008), *fpa-8* (Bäurle et al., 2007), *ibm1-1* (Saze et al., 2008), *ibm2-1* (Saze et al., 2013), the triple *suvh456* mutant (Ebbs and Bender, 2006), *cmt3-11 ibm2-5* (Coustham et al., 2014), and *kyp ibm2-5* (Coustham et al., 2014). The following lines were previously described: the transgenic *fpa-8* line (Col-0 background) carrying a *35S:FPA-YFP* construct (Bäurle et al., 2007) and the *ibm1-3* complemented lines expressing a *35S:YFP-IBM1-L* cDNA (Fan et al., 2012).

For ethylmethane sulfonate (EMS) mutagenesis, ~ 7,000 *ibm2-4* seeds were incubated in water containing 0.1% (v/v) EMS for 15 hours at room temperature and washed several times with water. Plants were then grown in pools of 16 (440 M1 pools in total) in greenhouses in long-day conditions at 20°C. The next generation was obtained by growing 200 M2 plants per pool that were selfed to obtain the M3 generation. The genetic screen was performed on M3s.

Seeds of plants grown *in vitro* were first surface sterilized and then sown on Gamborg B5 medium containing 1% (w/v) Sucrose. Plants were cultivated in growth chambers at 21°C in long day conditions.

Gene expression analyses

Total RNA was isolated from the aerial parts of 21-day-old seedlings grown *in vitro* using the RNeasy Plant Mini kit (*Qiagen*) followed by a DNAse treatment (*Fermentas*). RT-PCR was performed on 500 ng (except for *RPP7* amplifications where 1 µg was used) of total RNAs with the M-MLV reverse transcriptase (*Fermentas*), and cDNAs were diluted 10 times. Five µl was used for RT-qPCR using a CFX96 real-time PCR machine (*BioRad*) with a SYBR solution (*Eurogentec*) and primers listed in Supplemental Table S4. Expression levels were normalized against the Arabidopsis *UBC21* gene (*AT5G25760*).

Pathogen infection assays

To test *RPP7* disease resistance function, plants were inoculated with *Hyaloperonospora arabidopsidis (Hpa)* isolate Hiks1, which is an oomycete pathogen specifically recognized by *RPP7* in Arabidopsis accession Col-0 and virulent on accession Ksk-1 (Slusarenko and Schlaich, 2003). The function of another *Hpa* resistance gene, *RPP4*, was assessed by inoculating the plants with *Hpa* isolate EMWA1, which is specifically recognized by *RPP4* in Arabidopsis accession Col-0 and virulent on the Col-0 *eds1-2* mutant (García et al.,

2010). Briefly, 14-day-old plants were sprayed with water containing 4 x 10^4 *Hpa* Hiks1 spores per ml. Plant cell necrosis and Hiks1 or EMWA1 hyphal development were monitored by staining leaves with lactophenol trypan blue as described (Koch and Slusarenko, 1990). Stained leaves were viewed under a binocular light microscope. Infection assays were repeated independently at least three times with similar results.

Whole-genome sequencing and bioinformatic analyses

The genomes of *fpa-11 ibm2-4* and *ibm2-4* were sequenced using HiSeq technology (*Illumina*). Mutations were identified using the *MutDetect* pipeline described previously (Girard et al., 2014).

For *fpa-3*, *fpa-8 35S:FPA-YFP*, and *fpa-11 ibm2-4* methylome sequencings, bisulfite treatment, library preparation, and whole-genome sequencing (final depth of 20X) were performed by the BGI (China) using HiSeq technology (*Illumina*) producing 100 bp paired-end reads (Supplemental Table S1). Reads were trimmed with *Trim_Galore* (*Babraham Bioinformatics*) and aligned to the Col-0 Arabidopsis TAIR10 reference genome with *Bismark* version 0.14.5 (*Babraham Bioinformatics*) using standard options (*Bowtie2*; 1 mismatch allowed). Identical pairs were collapsed. Subsequent analyses were done using the following R packages: *bsseq* version 1.7.7 (Hansen et al., 2012) and *DSS* version 2.11.3 (Wu et al., 2015) to call Differentially-Methylated Regions (DMRs) as previously described (Corem et al., 2018). The hcDMR pipeline was used as indicated (Zhang et al., 2018) to filter spontaneous DMRs occurring in Arabidopsis Col-0 bisulfite sequencings. DMRs arising in *fpa* and restored to wild-type patterns in *fpa* complemented lines corresponded to DMRs found between *fpa-3* and the corresponding Col-0 controls that overlapped with DMRs found between *fpa-3* and the *fpa* complemented line but not with DMRs found between the *fpa* complemented line and its Col-0 control. DMRs that remained differentially methylated when the FPA function was restored corresponded to DMRs found between *fpa-3* and the corresponding Col-0 controls that overlapped with DMRs found between the *fpa* complemented line and its Col-0 control.

For DRS analyses, we retrieved the data corresponding to the study PRJEB3993 deposited at the ENA (Duc et al., 2013). Raw DRS reads were aligned using *TopHat2* (Kim et al., 2013), allowing a maximum of two mismatches and no gaps.

For transposon expression analyses, we used *ibm2* and *aipp1* RNA-seq data described previously (Stroud et al., 2012; Saze et al., 2013; Wang et al., 2013; Duan et al., 2017). Reads were trimmed with *Trim_Galore* (*Babraham Bioinformatics*) and aligned to the Col-0 Arabidopsis TAIR10 reference genome with *HISAT2* version 2.1.0 (Kim et al., 2015) using

standard options. Differential expression analyses were done with *DESeq2* version 1.20.0 (Love et al., 2014) in R version 3.5.1. To define transposon transcripts differently expressed, we used a significance cut-off of 0.05 and a 2-fold change relative to wild type. RNA-seq read coverage files were produced and normalized with *deepTools2* (Ramírez et al., 2018).

Targeted bisulfite sequencing

For each sample, 1 to 2 µg of genomic DNA was extracted from leaves corresponding to bulks of 10 to 15 plants, using the NucleoSpin Plant II kit (*Macherey-Nagel*). DNA was treated with bisulfite using the EpiTect Bisulfite Kit (*Qiagen*). Treated DNA was amplified using primers listed in Supplemental Table S4. PCR fragments were then cloned in pTOPO (*Life Technologies*) and sequenced individually. Results were analyzed with the Kismeth tool (Gruntman et al., 2008).

ACCESSION NUMBERS

WGBS data described in this study are available from the ENA database under the accession number PRJEB28432.

SUPPLEMENTAL DATA

Supplemental Figure S1. Expression analysis of two IBM2 targets in *cmt3 ibm2* and *kyp ibm2*

Supplemental Figure S2. Late flowering phenotype of *fpa-11 ibm2-4* and *fpa-3 ibm2-4* mutants

Supplemental Figure S3. *ibm2-4* suppressor screen

Supplemental Figure S4. CG and CHH methylation levels of genes in *ibm2* and *fpa ibm2* mutants.

Supplemental Figure S5. Schematic representation of the IBM2 target genes and localization of the regions amplified by qPCR

Supplemental Figure S6. Characterization of plants overexpressing *FPA* or *IBM1*

Supplemental Figure S7. Expression of IBM2 non-intronic target transposons

Supplemental Figure S8. Host responses and *Hpa* EMWA1 growth in Arabidopsis mutant lines

Supplemental Figure S9. Methylation patterns of the *IBM1* intron in *ibm2* and *fpa* mutants

Supplemental Figure S10. Methylation of *IBM1* intron in *fpa* determined by whole-genome sequencing after bisulfite conversion

Supplemental Figure S11. Methylation profiles of transposons derepressed in *fpa*

Supplemental Table S1. Bisulfite sequencing statistics

Supplemental Table S2. List of transposons differentially expressed in *ibm2*, *edm2*, and *aipp1*

Supplemental Table S3. DMRs identified between *fpa-3* and the wild type in CG, CHG, and CHH contexts

Supplemental Table S4. List of primers

ACKNOWLEDGMENTS

The authors wish to thank Eric Kemen (MPIPZ) for providing Ksk-1 seeds, Thomas Eulgem (UC Riverside) for *Hpa* isolate Hiks1, Caroline Dean for the *35S:FPA-YFP* line, and Ligeng Ma for the *35S:YFP-IBM1* line. We acknowledge funding from the Agence Nationale de la Recherche (Project 11-JSV7-0013) to NB, the Max-Planck Society and a H2020-Marie Skłodowska-Curie Actions Individual Fellowship (705631-CHERI) to CLR and JEP. The Institut Jean-Pierre Bourgin benefits from the support of the LabEx Saclay Plant Sciences-SPS (Project 10-LABX-0040-SPS). We are grateful to the *Genotoul* bioinformatics platform Toulouse Midi-Pyrénées for providing help and computing resources.

LEGENDS OF FIGURES

Figure 1. Phenotype of the *ibm2* suppressor

(A) Wild type (Col-0), *ibm2-4*, and the *ibm2* suppressor (*fpa-11 ibm2-4*) plants were grown in the greenhouse and pictured after 25 days. Scale bar = 1 cm.

(B) CHG methylation levels of genes in *ibm2-4* and *fpa-11 ibm2-4* mutants. The average methylation levels of genes were determined by dividing the genes into 100 bp bins. Regions located 1 kb upstream and 1 kb downstream are shown.

(C) Total number of DMRs found in the three methylation contexts (mCG, mCHG, and mCHH). Hypo- and hypermethylated DMRs are shown.

Figure 2. Expression analyses of IBM2 target genes in *fpa* mutants

The expression of IBM2 targets were determined by RT-qPCR in *ibm2-4*, *fpa-3*, and *fpa-11* back-crossed twice to Col-0 and the double *ibm2-4 fpa-11* and *ibm2-4 fpa-3* mutants. Results were normalized to Col-0 (expression fixed at 1 for each experiment). The PCR fragments amplified are shown in Supplemental Figure S5. Error bars represent SD (n=9). The asterisks indicate a significant difference between the sample and the corresponding Col-0 control determined by Student's *t*-test (* $p<0.05$; ** $p<0.01$; *** $p<0.001$).

Figure 3. Reduced expression of IBM2 target genes in plants over-expressing *FPA*

Expression analysis of *RPP7*, *IBM1*, *AT1G11270*, and *AT3G05410* transcript isoforms in an *fpa-8* mutant complemented by a *35S:YFP-FPA* construct resulting in the over-expression of *FPA* (Supplemental Figure S6). The expression was determined by RT-qPCR using primers (Supplemental Table S4) specific of IBM2 targets as shown in Supplemental Figure S5. Error bars represent SD (n=9). The asterisks indicate a significant difference between the sample and the corresponding Col-0 control determined by Student's *t*-test (*** $p<0.001$).

Figure 4. Host *RPP7* resistance and *Hpa* Hiks1 growth in Arabidopsis mutant lines

Two-week-old seedlings of the indicated genotypes were inoculated with *Hpa* Hiks1 (see Materials and Methods). At 4 days after inoculation, the two first true leaves of >10 plants per genotype were stained with lactophenol trypan blue to reveal necrotic plant cells and pathogen structures. *Hpa* Hiks1 is recognized by resistance gene *RPP7*. Col-0 expressing *RPP7* is resistant and Ksk-1 lacking *RPP7* is susceptible to *Hpa* Hiks1 infection. *Hpa* Hiks1 hyphal growth is restricted at HR sites in Col-0 whereas hyphae ramify through Ksk-1 leaves. Col-0

ibm2-1 or *ibm2-4* and Col-0 *suvh456* display reduced *RPP7* resistance to *Hpa* Hiks1. EDM2 is regulating *RPP7* transcript levels and Col-0 *edm2-4* mutants are therefore susceptible to *Hpa* Hiks1 (Eulgem et al., 2007). *fpa-11 ibm2-4* double mutant exhibits intermediate *RPP7* resistance. Col-0 *fpa-3* or *fpa-11* mutants and Col-0 *ibm1-1* are not affected in *RPP7* resistance. Plants shown were grown and inoculated at the same time. Similar results were obtained in three independent experiments. *HR*, host hypersensitive response; *h*, *Hpa* Hiks1 hyphae; *Sp*, *Hpa* Hiks1 sporangiophore. Scale bars = 1 mm.

Figure 5. Polyadenylation of IBM2 intronic targets

Reads corresponding to the direct RNA sequencing (DRS) of *fpa-7* and the Col-0 wild type (Duc et al., 2013) were aligned to the sequence of Col-0 (TAIR10 version).

(A) DRS reads for *IBM1, AT3G05410,* and *RPP7* loci were visualized using the *Integrated Genome Browser* (IGB). Proximal (*Prox.*) and distal (*Dist.*) polyadenylation sites are indicated. Each biological repeat is presented individually (rep#1 to #3). The scale is identical for all repeats presented for a given gene. The gene model is shown with exons represented by black boxes.

(B) DRS reads mapping the proximal or distal polyadenylation site regions were counted and normalized in reads per million mapped reads (RPM). Error bars represent SD (n=3). The asterisks indicate a significant difference between the sample and the Col-0 control determined by Student's *t*-test (* $p<0.05$; ** $p<0.01$).

Figure 6. Expression analysis of IBM2 non-intronic target transposons

(A**)** Schematic representation of the *Copia* (*AT4G16870*) - *RPP4* (*AT4G16860*) locus targeted by IBM2. The exons of *RPP4* are in blue, and the *Copia* element is in green.

(B) Expression analysis of *RPP4*, *AT4G16870*, and the chimeric *RPP4-AT4G16870* transcripts in Col-0 and different mutant backgrounds. cDNAs were amplified using primers indicated in (A) and described previously (Wang and Warren, 2010). *ATEF* cDNA amplifications served as controls.

(C) Expression analysis of *AT4TE21110* in Col-0 wild type and different mutant backgrounds. *AT4TE21110* is localized in the pericentromeric region of chromosome 4. RNAs were extracted from bulks (#1 and #2) of 20 plants grown *in vitro* for 15 days and cDNAs were amplified using primers described in Supplemental Table S4. *ACTIN* cDNA amplifications served as controls.

Figure 7. Methylation of *IBM1* intron in *fpa* mutants and an *IBM1* overexpressing line

(A) The methylation levels within the large intron of *IBM1*, in the region containing the heterochromatic marks (chromosome 3, position 2,430,285 to 2,430,595), are indicated. Data were obtained by amplifying the region after bisulfite conversion and correspond to the average methylation ratio determined between the repeats (Supplemental Figure S9).
(B) Methylation on top (positive values) and bottom (negative values) strands across the coding sequence of *IBM1* in *fpa-3*. The *IBM1* gene model is shown according to TAIR10. Mean methylation levels per cytosine are plotted on a 0 to 100% scale for each strand. Data correspond to the combination of two biological repeats for each genotype. CG methylation is in red, CHG in blue, and CHH in green. The CHG hypoDMR identified between *fpa-3* and Col-0 is represented by a blue rectangle.

Figure 8. Patterns of methylation in *fpa*
(A) Pairwise comparison of methylation in wild type and *fpa-3* mutants. Each dot represents a 100 bp-window, and their methylation levels were determined as follows. The Arabidopsis genome (TAIR10 release) was partitioned in 100 bp-tiles and methylation levels correspond to the ratios of methylated cytosines over the total number of cytosines. Only cytosines covered by at least five reads were considered. The average methylation levels were determined by combining the two biological replicates for each genotype. The color scale measures the density of points (red being very dense). The Pearson correlation coefficients between the samples are 0.97 for mCG, 0.98 for mCHG and 0.94 for mCHH.
(B) Nature of CG hypo- and hyperDMRs identified in *fpa-3*. '*gene+TE*' corresponds to DMRs overlapping with both genes and transposons, '*gene*' corresponds to DMRs overlapping with genes, and '*TE*' corresponds to DMRs overlapping with transposons. All other DMRs were classified as '*Intergenic*'.
(C) Methylation levels of CG hypo- and hyperDMRs. The average methylation levels of the DMRs were determined by dividing the DMR into 100 bp bins. Regions located 1 kb upstream and 1 kb downstream are shown.

LEGENDS OF SUPPLEMENTARY MATERIALS

Supplemental Figure S1. Expression analysis of two IBM2 targets in *cmt3 ibm2* and *kyp ibm2*

RT-qPCR analyses of *RPP7-L* and *AT3G05410-L* expression in Col-0, *ibm2-4*, *cmt3-11 ibm2-5* (Coustham et al., 2014) and *kyp ibm2-5* (Coustham et al., 2014). Results were normalized to Col-0 (expression fixed at 1 for each experiment). Error bars represent SD (n=4).

Supplemental Figure S2. Late flowering phenotype of *fpa-11 ibm2-4* and *fpa-3 ibm2-4* mutants

Supplemental Figure S3. ***ibm2-4* suppressor screen**

Expression analyses of an IBM2 target in 9 M3 plants (#1 to #9) retrieved from the *ibm2-4* suppressor screen. RNAs of plants were extracted and cDNAs were amplified using primers corresponding to *AT3G05410-L* (Supplemental Figure S5). *ATEF* amplifications served as controls. The GeneRuler DNA Ladder Mix (Ref SM0331, *Thermo*) is the DNA ladder used.

Supplemental Figure S4. **CG and CHH methylation levels of genes in *ibm2* and *fpa ibm2* mutants**

The average methylation levels of genes were determined by dividing the genes into 100 bp bins. Regions located 1 kb upstream and 1 kb downstream are shown.

Supplemental Figure S5. Schematic representation of the IBM2 target genes and localization of the regions amplified by RT-qPCR

Schematic representation of the IBM2 target gene drawn to scale. The region (chromosome 3, position 2,430,285 to 2,430,595) containing intronic heterochromatic marks in *IBM1* is represented by a blue bar.

Supplemental Figure S6. Characterization of plants overexpressing *FPA* or *IBM1*

RNAs were extracted from bulks of plants carrying the *35S:FPA-YFP* or *35S:YFP-IBM1* constructs. Both *FPA* (A) or *IBM1-L* (B) cDNAs were amplified using specific primers (Supplemental Table S4). *ATEF* or *ACTIN* cDNA amplifications served as controls.

Supplemental Figure S7. Expression of IBM2 non-intronic target transposons

RNA-seq data were retrieved from the following GEO projects: GSE38286 for *suvh456* and the three corresponding wild-type repeats (Stroud et al., 2012), GSE98655 for *aipp1-1*, *edm2-4*, *ibm2*/*asi1-2* and the two wild-type repeats (Duan et al., 2017), GSE48026 for *asi1-1* and the corresponding wild type (Wang et al., 2013) and PRJDB2180 for *ibm1-4*, *ibm2-2* and the wild type (Saze et al., 2013). The methylation levels for mCG, mCHG and mCHH are shown for the wild type and *fpa-3* plants. The screenshots were obtained with Integrative Genome Browser (IGB). The scales indicated on the left are identical for all RNA-seq or methylation tracks, respectively. *RPKM*; Reads Per Kilobase per Million mapped reads. (A) *RPP4* locus, (B) *AT4TE21110* locus.

Supplemental Figure S8. Host responses and *Hpa* EMWA1 growth in Arabidopsis mutant lines

Two-week-old seedlings of the indicated genotypes were inoculated with *Hpa* EMWA1 (see Materials & Methods). At 4 days after inoculation, the two first true leaves of >10 plants per genotype were stained with lactophenol trypan blue to reveal necrotic plant cells and pathogen structures. *Hpa* EMWA1 is specifically recognized by *RPP4*. Col-0 expressing *RPP4* is resistant and *eds1-2* mutants (García et al., 2010) are susceptible to *Hpa* EMWA1 infection. *Hpa* EMWA1 hyphal growth is restricted at HR sites in Col-0 whereas hyphae ramify through *eds1-2* leaves. None of the mutants (in the Col-0 background) are affected in *RPP4* resistance. Plants were grown and inoculated at the same time. Similar results were obtained in three independent experiments.

Supplemental Figure S9. Methylation patterns of the *IBM1* intron in *ibm2* and *fpa* mutants

After bisulfite conversion of DNAs, the region indicated in Supplemental Figure S5 (*IBM1*, blue bar) was amplified in the large intron of *IBM1* using primers described in Supplemental Table S4. Samples are corresponding to leaves from 10 to 15 plants bulked together. The number of clones sequenced (n) is indicated. Sequences were aligned and the methylation quantified using the Kismeth tool (Gruntman et al., 2008). Cytosines are represented by circles (red for CGs, blue for CHGs, green for CHHs; solid circles: methylated cytosines).

Supplemental Figure S10. Methylation of *IBM1* intron in *fpa* determined by whole-genome sequencing after bisulfite conversion

The methylation levels within the large intron of *IBM1*, in the region containing heterochromatic marks (chromosome 3, position 2,430,285 to 2,430,595), are indicated. Data for three wild-type (Col-0) repetitions, *fpa-7*, *fca-9 fpa-7* and *suvh4* were obtained from raw data publicly available (Stroud et al., 2013). Data for *ibm2-4* and the corresponding wild type (Col-0) were obtained from our previous methylome sequencing data (Coustham et al., 2014).

Supplemental Figure S11. Methylation profiles of transposons derepressed in *fpa*

Mean methylation levels for mCG, mCHG and mCHH were obtained by combining the two biological replicates for the wild type or *fpa-3*, respectively. The screenshots were obtained with Integrative Genome Browser (IGB). HypoDMRs between the mutant and the wild type are contained in the boxed area. The scale is identical for all tracks.

Supplemental Table S1. *B*isulfite sequencing statistics

Col #1, biological replicate #1 Col-0 methylome sequencing; Col #2, biological replicate #2 Col-0 methylome sequencing; *fpa-3* #1, biological replicate #1 *fpa-3* mutant methylome sequencing; *fpa-3* #2, biological replicate #1 *fpa-3* mutant methylome sequencing; *35S:FPA-YFP*, *35S:FPA-YFP* methylome sequencing ; Col-0 (*35S:FPA-YFP* control), Col-0 methylome sequencing; *fpa-11 ibm2-4*, *fpa ibm2* methylome sequencing. To determine the bisulfite conversion rates, reads were aligned to the TAIR10 Arabidopsis chloroplast sequence.

Supplemental Table S2. Transposons differentially expressed in *ibm2*, *edm2* and *aipp1* compared to wild type

The IBM2 targets previously identified are in red.

Supplemental Table S3. DMRs identified between *fpa-3* and the wild type in CG, CHG and CHH contexts

DMRs were defined using two biological repeats per genotype with the *bsseq* and *DSS* R packages (see Materials & Methods).

Supplemental Table S4. List of primers

REFERENCES

Bäurle I, Smith L, Baulcombe DC, Dean C (2007) Widespread role for the flowering-time regulators FCA and FPA in RNA-mediated chromatin silencing. Science **318:** 109-112

Corem S, Doron-Faigenboim A, Jouffroy O, Maumus F, Arazi T, Bouché N (2018) Redistribution of CHH methylation and small interfering RNAs across the genome of tomato *ddm1* mutants. Plant Cell **7:**1628-1644

Coustham V, Vlad D, Deremetz A, Gy I, Cubillos FA, Kerdaffrec E, Loudet O, Bouché N (2014) SHOOT GROWTH1 maintains Arabidopsis epigenomes by regulating IBM1. PLoS One **9:** e84687

Du J, Johnson LM, Groth M, Feng S, Hale CJ, Li S, Vashisht AA, Gallego-Bartolome J, Wohlschlegel JA, Patel DJ, Jacobsen SE (2014) Mechanism of DNA methylation-directed histone methylation by KRYPTONITE. Mol Cell **55:** 495-504

Du J, Zhong X, Bernatavichute YV, Stroud H, Feng S, Caro E, Vashisht AA, Terragni J, Chin HG, Tu A, Hetzel J, Wohlschlegel JA, Pradhan S, Patel DJ, Jacobsen SE (2012) Dual binding of chromomethylase domains to H3K9me2-containing nucleosomes directs DNA methylation in plants. Cell **151:** 167-180

Duan CG, Wang X, Zhang L, Xiong X, Zhang Z, Tang K, Pan L, Hsu CC, Xu H, Tao WA, Zhang H, Zhu JK (2017) A protein complex regulates RNA processing of intronic heterochromatin-containing genes in Arabidopsis. Proc Natl Acad Sci U S A **114:** E7377-e7384

Duc C, Sherstnev A, Cole C, Barton GJ, Simpson GG (2013) Transcription termination and chimeric RNA formation controlled by *Arabidopsis thaliana* FPA. PLoS Genet **9:** e1003867

Ebbs ML, Bender J (2006) Locus-specific control of DNA methylation by the Arabidopsis SUVH5 histone methyltransferase. Plant Cell **18:** 1166-1176

Eulgem T, Tsuchiya T, Wang XJ, Beasley B, Cuzick A, Tor M, Zhu T, McDowell JM, Holub E, Dangl JL (2007) EDM2 is required for RPP7-dependent disease resistance in Arabidopsis and affects RPP7 transcript levels. Plant J **49:** 829-839

Fan D, Dai Y, Wang X, Wang Z, He H, Yang H, Cao Y, Deng XW, Ma L (2012) IBM1, a JmjC domain-containing histone demethylase, is involved in the regulation of RNA-directed DNA methylation through the epigenetic control of RDR2 and DCL3 expression in Arabidopsis. Nucleic Acids Res **40:** 8905-8916

García AV, Blanvillain-Baufumé S, Huibers RP, Wiermer M, Li G, Gobbato E, Rietz S, Parker JE (2010) Balanced Nuclear and Cytoplasmic Activities of EDS1 Are Required for a Complete Plant Innate Immune Response. PLoS Pathog **6**

Girard C, Crismani W, Froger N, Mazel J, Lemhemdi A, Horlow C, Mercier R (2014) FANCM-associated proteins MHF1 and MHF2, but not the other Fanconi anemia factors, limit meiotic crossovers. Nucleic Acids Res **42:** 9087-9095

Gruntman E, Qi Y, Slotkin RK, Roeder T, Martienssen RA, Sachidanandam R (2008) Kismeth: Analyzer of plant methylation states through bisulfite sequencing. *In* BMC Bioinformatics, Vol 9. BioMed Central Ltd, p 371

Hansen KD, Langmead B, Irizarry RA (2012) BSmooth: from whole genome bisulfite sequencing reads to differentially methylated regions. Genome Biol **13:** R83

Hornyik C, Duc C, Rataj K, Terzi LC, Simpson GG (2010) Alternative polyadenylation of antisense RNAs and flowering time control. Biochem Soc Trans **38:** 1077-1081

Hornyik C, Terzi LC, Simpson GG (2010) The spen family protein FPA controls alternative cleavage and polyadenylation of RNA. Dev Cell **18:** 203-213

Inagaki S, Miura-Kamio A, Nakamura Y, Lu F, Cui X, Cao X, Kimura H, Saze H, Kakutani T (2010) Autocatalytic differentiation of epigenetic modifications within the Arabidopsis genome. EMBO J **29:** 3496-3506

Johnson LM, Bostick M, Zhang X, Kraft E, Henderson I, Callis J, Jacobsen SE (2007) The SRA methyl-cytosine-binding domain links DNA and histone methylation. Curr Biol **17:** 379-384

Kim D, Langmead B, Salzberg SL (2015) HISAT: a fast spliced aligner with low memory requirements. Nature Methods **12:** 357

Kim D, Pertea G, Trapnell C, Pimentel H, Kelley R, Salzberg SL (2013) TopHat2: accurate alignment of transcriptomes in the presence of insertions, deletions and gene fusions. Genome Biol **14:** R36

Koch E, Slusarenko A (1990) Arabidopsis is susceptible to infection by a downy mildew fungus. Plant Cell **2:** 437-445

Lai Y, Cuzick A, Lu XM, Wang J, Katiyar N, Tsuchiya T, Le Roch K, McDowell JM, Holub E, Eulgem T (2018) The Arabidopsis RRM domain protein EDM3 mediates race-specific disease resistance by controlling H3K9me2-dependent alternative polyadenylation of RPP7 immune receptor transcripts. Plant J doi:10.1111/tpj.14148

Le TN, Miyazaki Y, Takuno S, Saze H (2015) Epigenetic regulation of intragenic transposable elements impacts gene transcription in Arabidopsis thaliana. Nucleic Acids Res **43:** 3911-3921

Liu F, Marquardt S, Lister C, Swiezewski S, Dean C (2010) Targeted 3' processing of antisense transcripts triggers Arabidopsis FLC chromatin silencing. Science **327:** 94-97

Love MI, Huber W, Anders S (2014) Moderated estimation of fold change and dispersion for RNA-seq data with DESeq2. Genome Biol **15:** 550

Lyons R, Iwase A, Gansewig T, Sherstnev A, Duc C, Barton GJ, Hanada K, Higuchi-Takeuchi M, Matsui M, Sugimoto K, Kazan K, Simpson GG, Shirasu K (2013) The RNA-binding protein FPA regulates *flg22*-triggered defense responses and transcription factor activity by alternative polyadenylation. Sci Rep **3:** 2866

Macknight R, Duroux M, Laurie R, Dijkwel P, Simpson G, Dean C (2002) Functional significance of the alternative transcript processing of the Arabidopsis floral promoter FCA. Plant Cell **14:** 877-888

Michaels SD, Amasino RM (2001) Loss of FLOWERING LOCUS C activity eliminates the late-flowering phenotype of FRIGIDA and autonomous pathway mutations but not responsiveness to vernalization. Plant Cell **13:** 935-941

Miura A, Nakamura M, Inagaki S, Kobayashi A, Saze H, Kakutani T (2009) An Arabidopsis jmjC domain protein protects transcribed genes from DNA methylation at CHG sites. EMBO J **28:** 1078-1086

Ong-Abdullah M, Ordway JM, Jiang N, Ooi SE, Kok SY, Sarpan N, Azimi N, Hashim AT, Ishak Z, Rosli SK, Malike FA, Bakar NA, Marjuni M, Abdullah N, Yaakub Z, Amiruddin MD, Nookiah R, Singh R, Low ET, Chan KL, Azizi N, Smith SW, Bacher B, Budiman MA, Van Brunt A, Wischmeyer C, Beil M, Hogan M, Lakey N, Lim CC, Arulandoo X, Wong CK, Choo CN, Wong WC, Kwan YY, Alwee SS, Sambanthamurthi R, Martienssen RA (2015) Loss of Karma transposon methylation underlies the mantled somaclonal variant of oil palm. Nature **525:** 533-537

Patil DP, Chen CK, Pickering BF, Chow A, Jackson C, Guttman M, Jaffrey SR (2016) m6A RNA methylation promotes XIST-mediated transcriptional repression. Nature **537:** 369-373

Ramírez F, Ryan DP, Grüning B, Bhardwaj V, Kilpert F, Richter AS, Heyne S, Dündar F, Manke T (2018) deepTools2: a next generation web server for deep-sequencing data analysis. Nucleic Acids Research **44:** W160-5**.**

Rigal M, Kevei Z, Pelissier T, Mathieu O (2012) DNA methylation in an intron of the IBM1 histone demethylase gene stabilizes chromatin modification patterns. EMBO J **31:** 2981-2993

Saze H, Kitayama J, Takashima K, Miura S, Harukawa Y, Ito T, Kakutani T (2013) Mechanism for full-length RNA processing of Arabidopsis genes containing intragenic heterochromatin. Nat Commun **4:** 2301

Saze H, Shiraishi A, Miura A, Kakutani T (2008) Control of genic DNA methylation by a jmjC domain-containing protein in Arabidopsis thaliana. Science **319:** 462-465

Slusarenko AJ, Schlaich NL (2003) Downy mildew of Arabidopsis thaliana caused by Hyaloperonospora parasitica (formerly Peronospora parasitica). Mol Plant Pathol **4:** 159-170

Sonmez C, Bäurle I, Magusin A, Dreos R, Laubinger S, Weigel D, Dean C (2011) RNA 3' processing functions of Arabidopsis FCA and FPA limit intergenic transcription. Proc Natl Acad Sci U S A **108:** 8508-8513

Stroud H, Greenberg MV, Feng S, Bernatavichute YV, Jacobsen SE (2013) Comprehensive analysis of silencing mutants reveals complex regulation of the Arabidopsis methylome. Cell **152:** 352-364

Stroud H, Hale CJ, Feng S, Caro E, Jacob Y, Michaels SD, Jacobsen SE (2012) DNA methyltransferases are required to induce heterochromatic re-replication in Arabidopsis. PLoS Genet **8:** e1002808

Sun YW, Tee CS, Ma YH, Wang G, Yao XM, Ye J (2015) Attenuation of Histone Methyltransferase KRYPTONITE-mediated transcriptional gene silencing by Geminivirus. Sci Rep **5:** 16476

Tsuchiya T, Eulgem T (2013) An alternative polyadenylation mechanism coopted to the Arabidopsis RPP7 gene through intronic retrotransposon domestication. Proc Natl Acad Sci U S A **110:** E3535-3543

Tsuchiya T, Eulgem T (2013) Mutations in EDM2 selectively affect silencing states of transposons and induce plant developmental plasticity. Sci Rep **3:** 1701

Veley KM, Michaels SD (2008) Functional redundancy and new roles for genes of the autonomous floral-promotion pathway. Plant Physiol **147:** 682-695

Wang X, Duan CG, Tang K, Wang B, Zhang H, Lei M, Lu K, Mangrauthia SK, Wang P, Zhu G, Zhao Y, Zhu JK (2013) RNA-binding protein regulates plant DNA methylation by controlling mRNA processing at the intronic heterochromatin-containing gene IBM1. Proc Natl Acad Sci U S A **110:** 15467-15472

Wang YH, Warren JT, Jr. (2010) Mutations in retrotransposon AtCOPIA4 compromises resistance to Hyaloperonospora parasitica in *Arabidopsis thaliana*. Genet Mol Biol **33:** 135-140

Wu H, Xu T, Feng H, Chen L, Li B, Yao B, Qin Z, Jin P, Conneely KN (2015) Detection of differentially methylated regions from whole-genome bisulfite sequencing data without replicates. Nucleic Acids Res **43**:e141.

Wu Z, Ietswaart R, Liu F, Yang H, Howard M, Dean C (2016) Quantitative regulation of FLC via coordinated transcriptional initiation and elongation. Proc Natl Acad Sci U S A **113:** 218-223

Zhang Y, Harris CJ, Liu Q, Liu W, Ausin I, Long Y, Xiao L, Feng L, Chen X, Xie Y, Zhan L, Feng S, Li JJ, Wang H, Zhai J, Jacobsen SE (2018) Large-scale comparative epigenomics reveals hierarchical regulation of non-CG methylation in Arabidopsis. *In* Proc Natl Acad Sci U S A, **115:** 1069-1074

Zhang Y, Li X, Goodrich J, Wu C, Wei H, Yang S, Feng X (2016) Reduced function of the RNA-binding protein FPA rescues a T-DNA insertion mutant in the Arabidopsis *ZHOUPI* gene by promoting transcriptional read-through. Plant Mol Biol **91:** 549-561

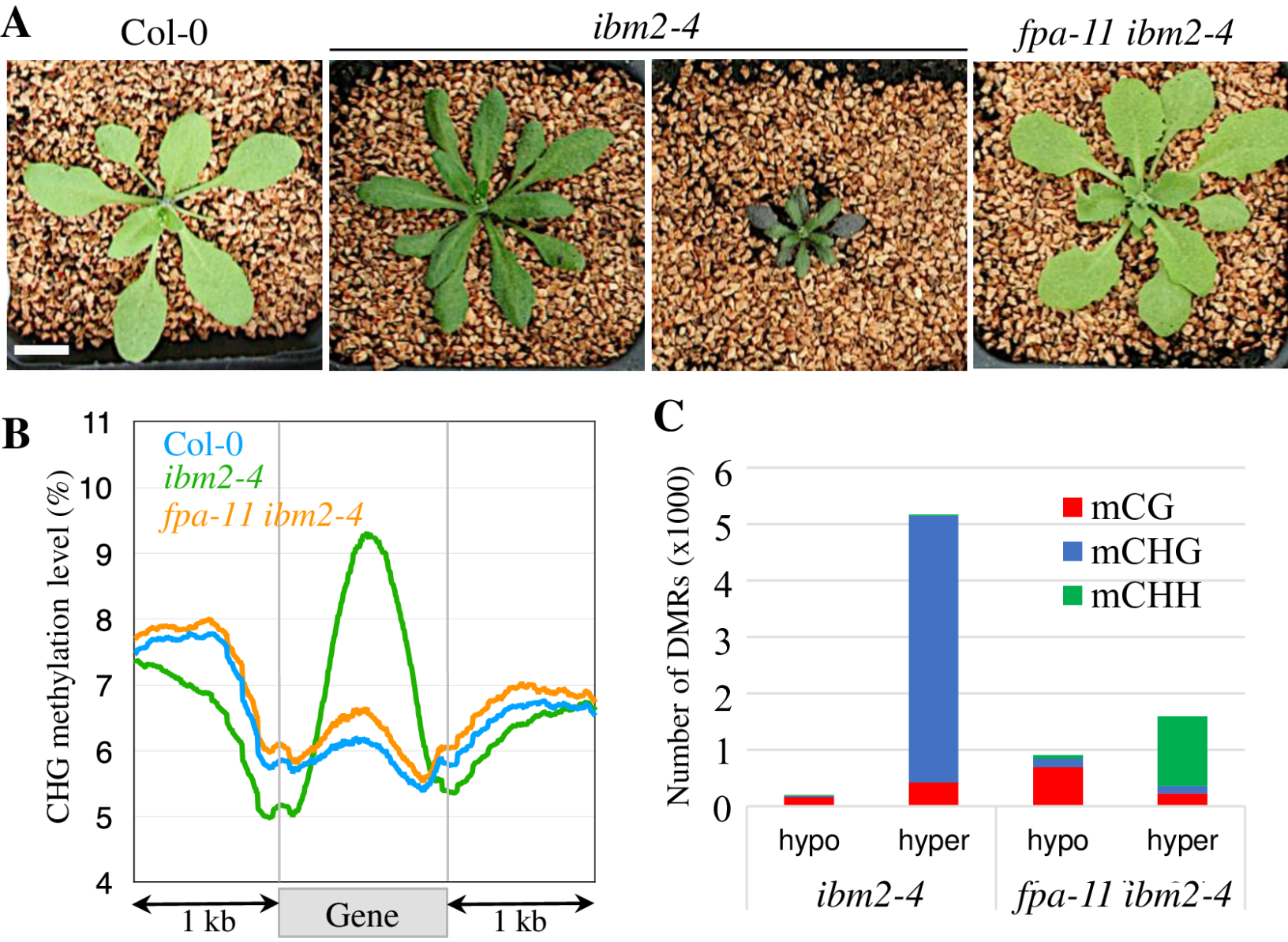

Figure 1. Phenotype of the *ibm2* suppressor

(A) Wild type (Col-0), *ibm2-4*, and the *ibm2* suppressor (*fpa-11 ibm2-4*) plants were grown in the greenhouse and pictured after 25 days. Scale bar = 1 cm.

(B) CHG methylation levels of genes in *ibm2-4* and *fpa-11 ibm2-4* mutants. The average methylation levels of genes were determined by dividing the genes into 100 bp bins. Regions located 1 kb upstream and 1 kb downstream are shown.

(C) Total number of DMRs found in the three methylation contexts (mCG, mCHG, and mCHH). Hypo- and hypermethylated DMRs are shown.

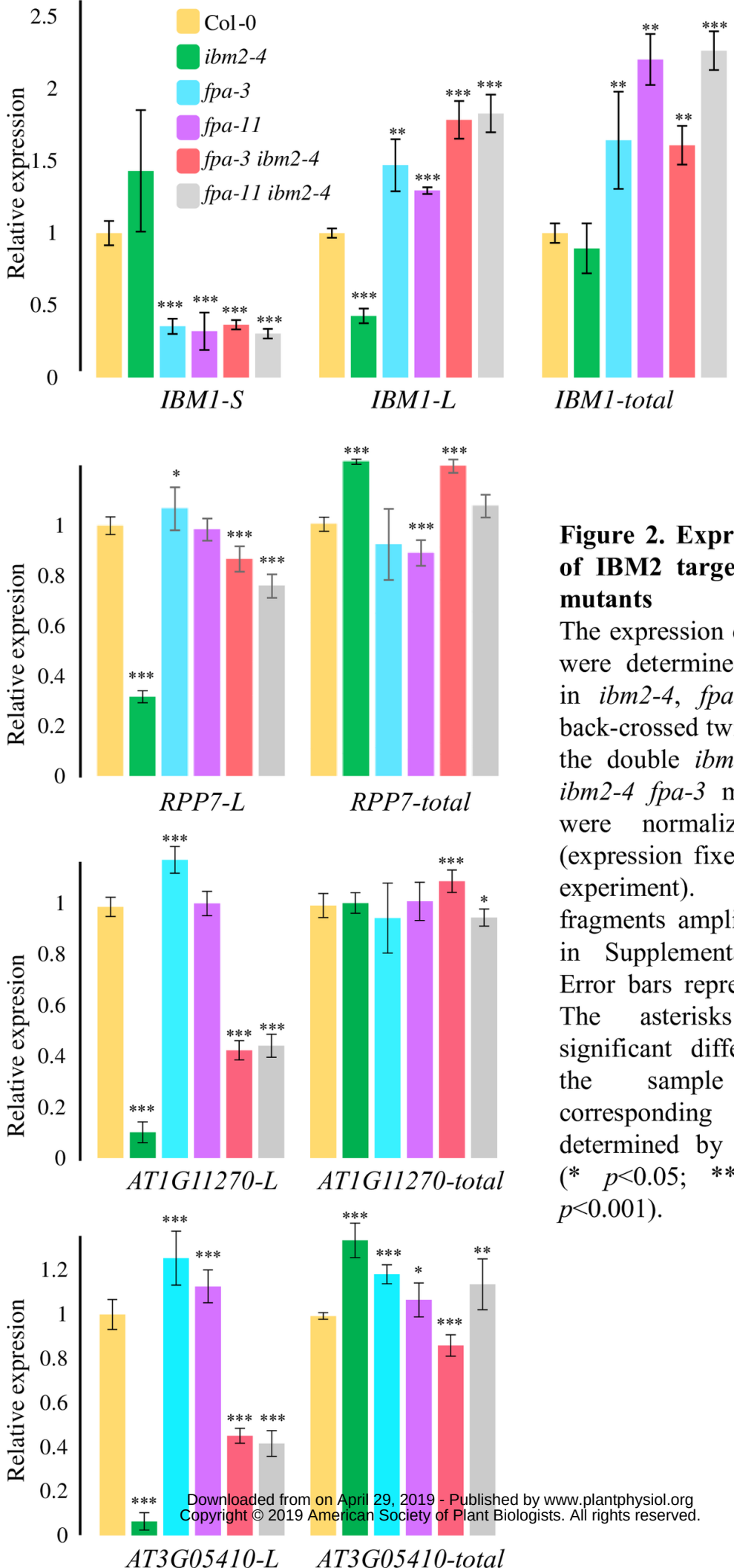

Figure 2. Expression analyses of IBM2 target genes in *fpa* mutants

The expression of IBM2 targets were determined by RT-qPCR in *ibm2-4*, *fpa-3*, and *fpa-11* back-crossed twice to Col-0 and the double *ibm2-4 fpa-11* and *ibm2-4 fpa-3* mutants. Results were normalized to Col-0 (expression fixed at 1 for each experiment). The PCR fragments amplified are shown in Supplemental Figure S5. Error bars represent SD (n=9). The asterisks indicate a significant difference between the sample and the corresponding Col-0 control determined by Student's *t*-test (* $p<0.05$; ** $p<0.01$; *** $p<0.001$).

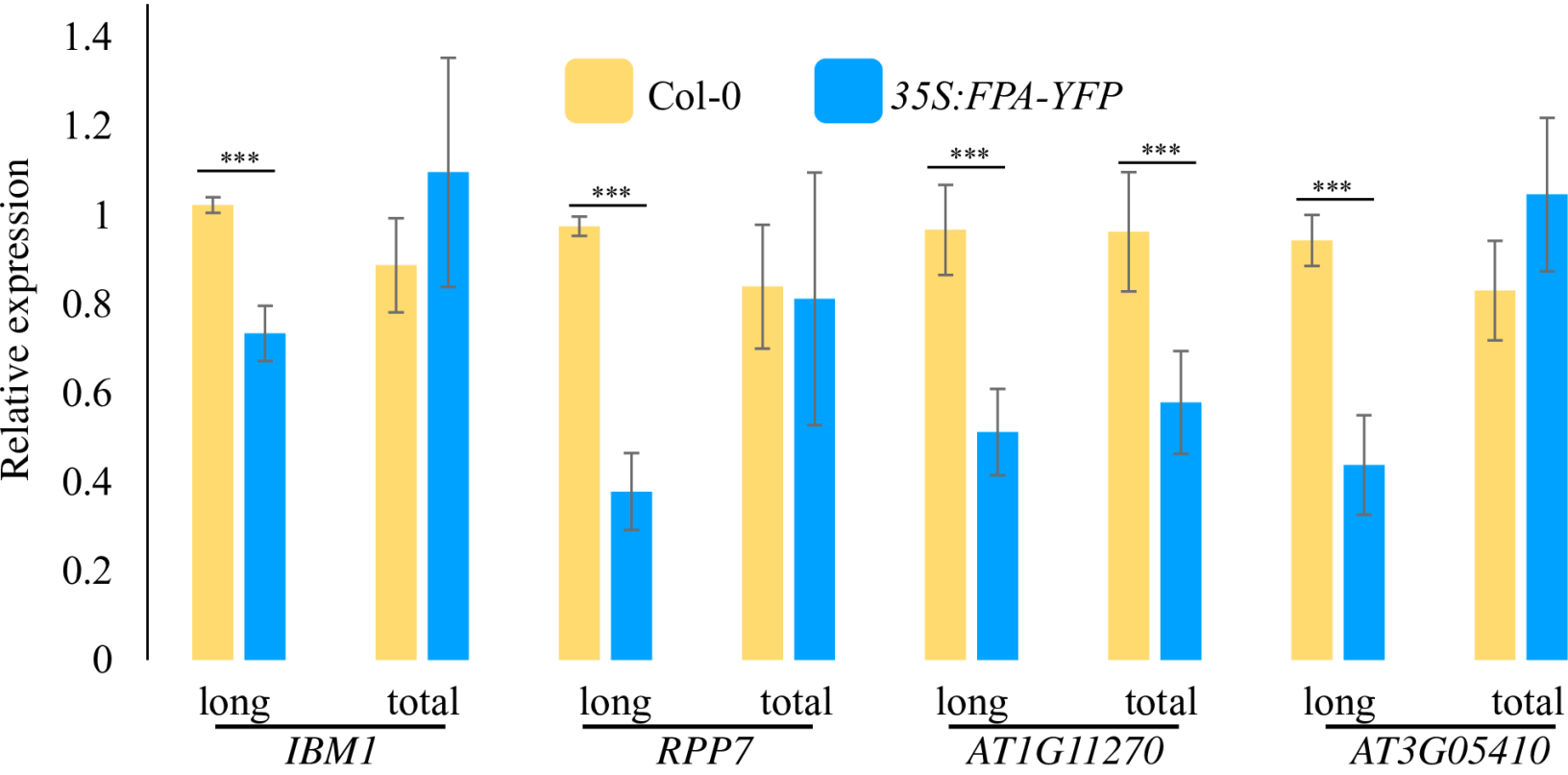

Figure 3. Reduced expression of IBM2 target genes in plants over-expressing *FPA*
Expression analysis of *RPP7*, *IBM1*, *AT1G11270*, and *AT3G05410* transcript isoforms in an *fpa-8* mutant complemented by a *35S:YFP-FPA* construct resulting in the over-expression of *FPA* (Supplemental Figure S6). The expression was determined by RT-qPCR using primers (Supplemental Table S4) specific of IBM2 targets as shown in Supplemental Figure S5. Error bars represent SD (n=9). The asterisks indicate a significant difference between the sample and the corresponding Col-0 control determined by Student's *t*-test (*** $p<0.001$).

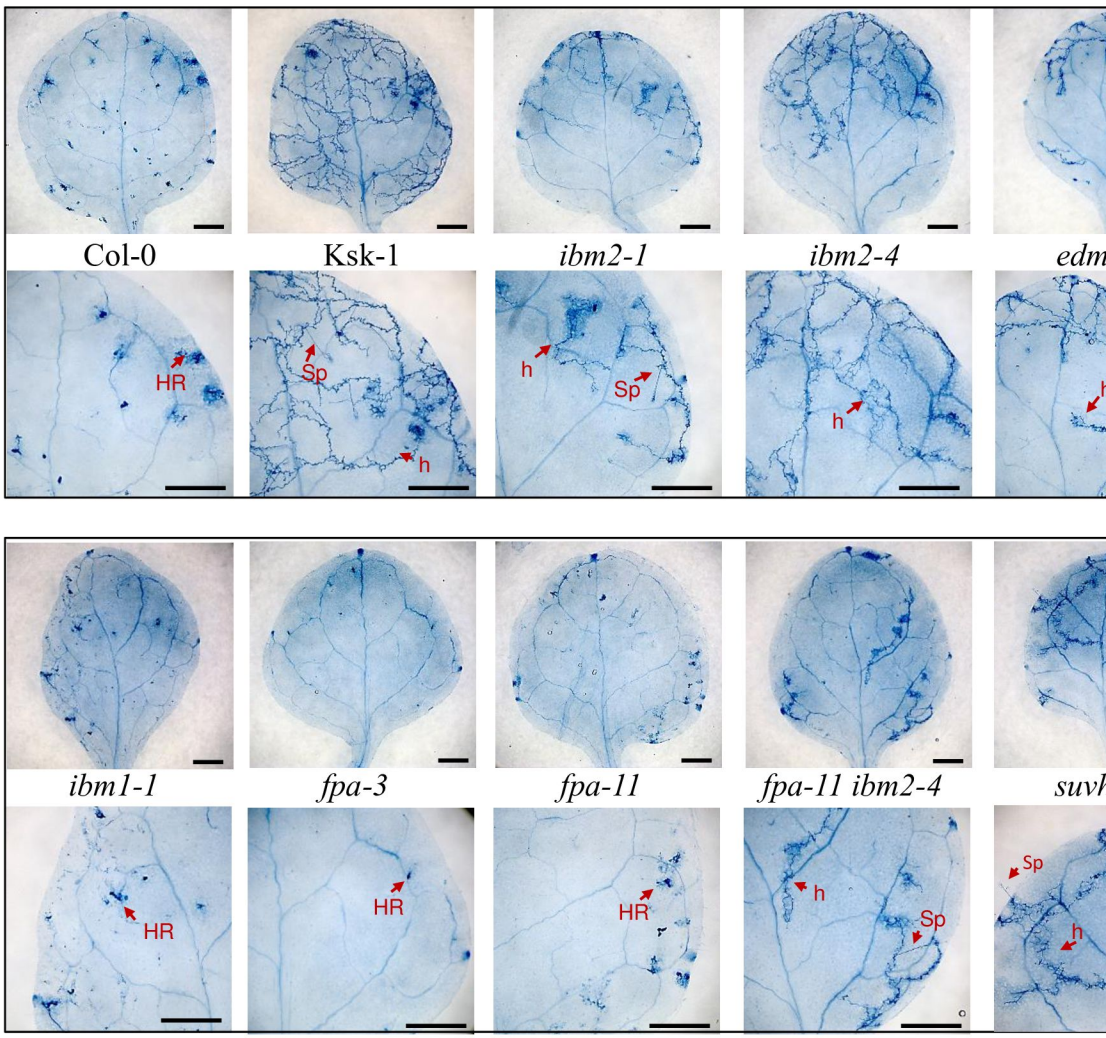

Figure 4. Host *RPP7* resistance and *Hpa* Hiks1 growth in Arabidopsis mutant lin
Two-week-old seedlings of the indicated genotypes were inoculated with *Hpa* Hik
Materials and Methods). At 4 days after inoculation, the two first true leaves of >1
per genotype were stained with lactophenol trypan blue to reveal necrotic plant ce
pathogen structures. *Hpa* Hiks1 is recognized by resistance gene *RPP7*. Col-0 exp
RPP7 is resistant and Ksk-1 lacking *RPP7* is susceptible to *Hpa* Hiks1 infection. *Hp*
hyphal growth is restricted at HR sites in Col-0. Photos: hyphae; h: haustoria; Sp
leaves. Col-0 *ibm2-1* or *ibm2-4* and Col-0 *suvh456* display reduced *RPP7* resistance
Hiks1. EDM2 is regulating *RPP7* transcript levels and Col-0 *edm2-4* mutants are th

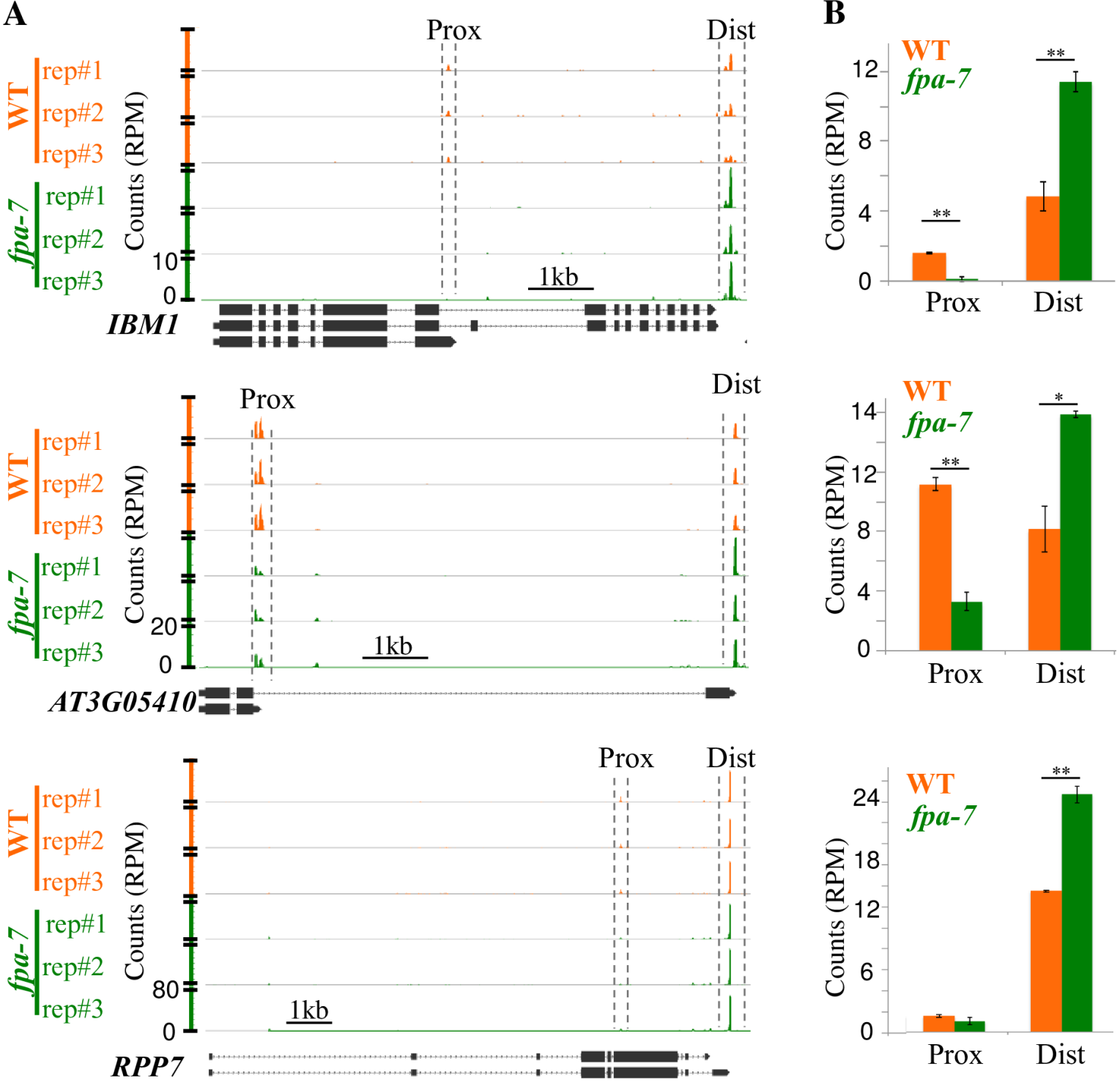

Figure 5. Polyadenylation of IBM2 intronic targets

Reads corresponding to the direct RNA sequencing (DRS) of *fpa-7* and the Col-0 wild type (Duc et al., 2013) were aligned to the sequence of Col-0 (TAIR10 version).

(A) DRS reads for *IBM1*, *AT3G05410*, and *RPP7* loci were visualized using the *Integrated Genome Browser* (IGB). Proximal (*Prox.*) and distal (*Dist.*) polyadenylation sites are indicated. Each biological repeat is presented individually (rep#1 to #3). The scale is identical for all repeats presented for a given gene. The gene model is shown with exons represented by black boxes.

(B) DRS reads mapping the proximal or distal polyadenylation site regions were counted and normalized in reads per million mapped reads (RPM). Error bars represent SD (n=3). The asterisks indicate a significant difference between the sample and the Col-0 control determined by Student's *t*-test (* $p<0.05$; ** $p<0.01$).

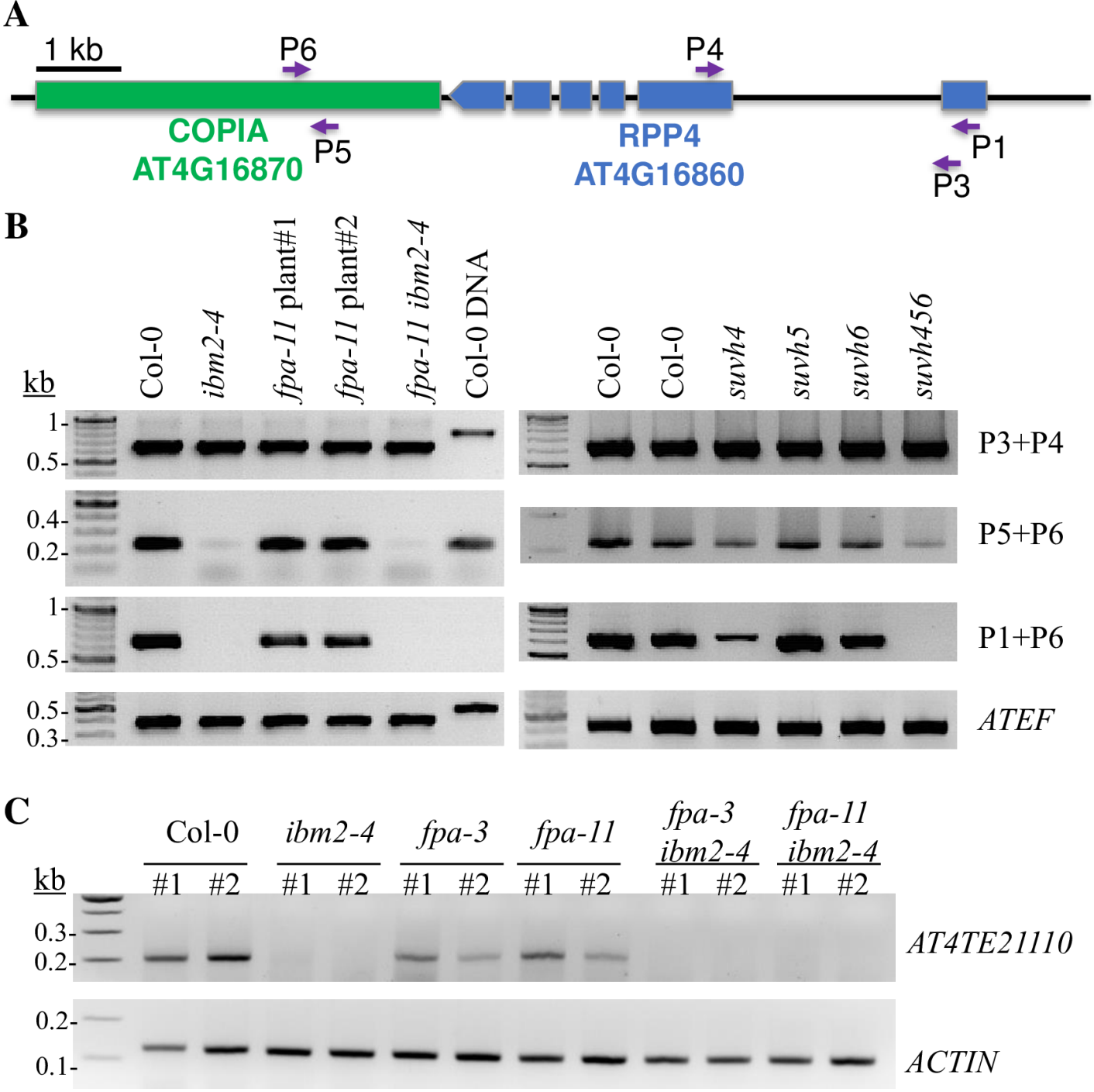

Figure 6. Expression analysis of IBM2 non-intronic target transposons

(A) Schematic representation of the *Copia* (*AT4G16870*) - *RPP4* (*AT4G16860*) locus targeted by IBM2. The exons of *RPP4* are in blue, and the *Copia* element is in green.

(B) Expression analysis of *RPP4*, *AT4G16870*, and the chimeric *RPP4-AT4G16870* transcripts in Col-0 and different mutant backgrounds. cDNAs were amplified using primers indicated in (A) and described previously (Wang and Warren, 2010). *ATEF* cDNA amplifications served as controls.

(C) Expression analysis of *AT4TE21110* in Col-0 wild type and different mutant backgrounds. *AT4TE21110* is localized in the pericentromeric region of chromosome 4. RNAs were extracted from bulks (#1 and #2) of 20 plants grown *in vitro* for 15 days and cDNAs were amplified using primers described in Supplemental Table S4. *ACTIN* cDNA amplifications served as controls.

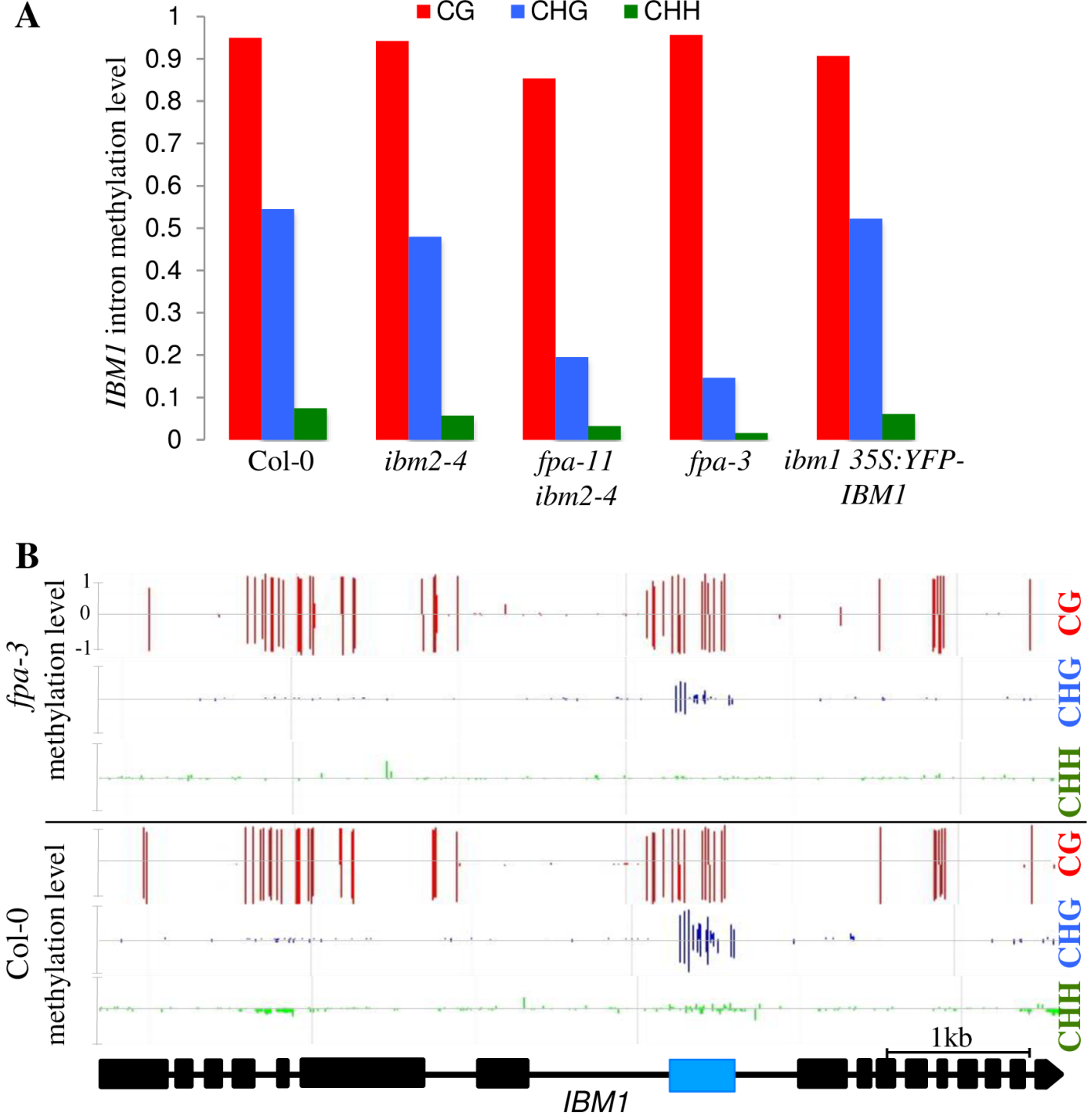

Figure 7. Methylation of *IBM1* intron in *fpa* mutants and an *IBM1* overexpressing line

(A) The methylation levels within the large intron of *IBM1*, in the region containing the heterochromatic marks (chromosome 3, position 2,430,285 to 2,430,595), are indicated. Data were obtained by amplifying the region after bisulfite conversion and correspond to the average methylation ratio determined between the repeats (Supplemental Figure S9).

(B) Methylation on top (positive values) and bottom (negative values) strands across the coding sequence of *IBM1* in *fpa-3*. The *IBM1* gene model is shown according to TAIR10. Mean methylation levels per cytosine are plotted on a 0 to 100% scale for each strand. Data correspond to the combination of two biological repeats for each genotype. CG methylation is in red, CHG in blue, and CHH in green. The CHG hypoDMR identified between *fpa-3* and Col-0 is represented by a blue rectangle.

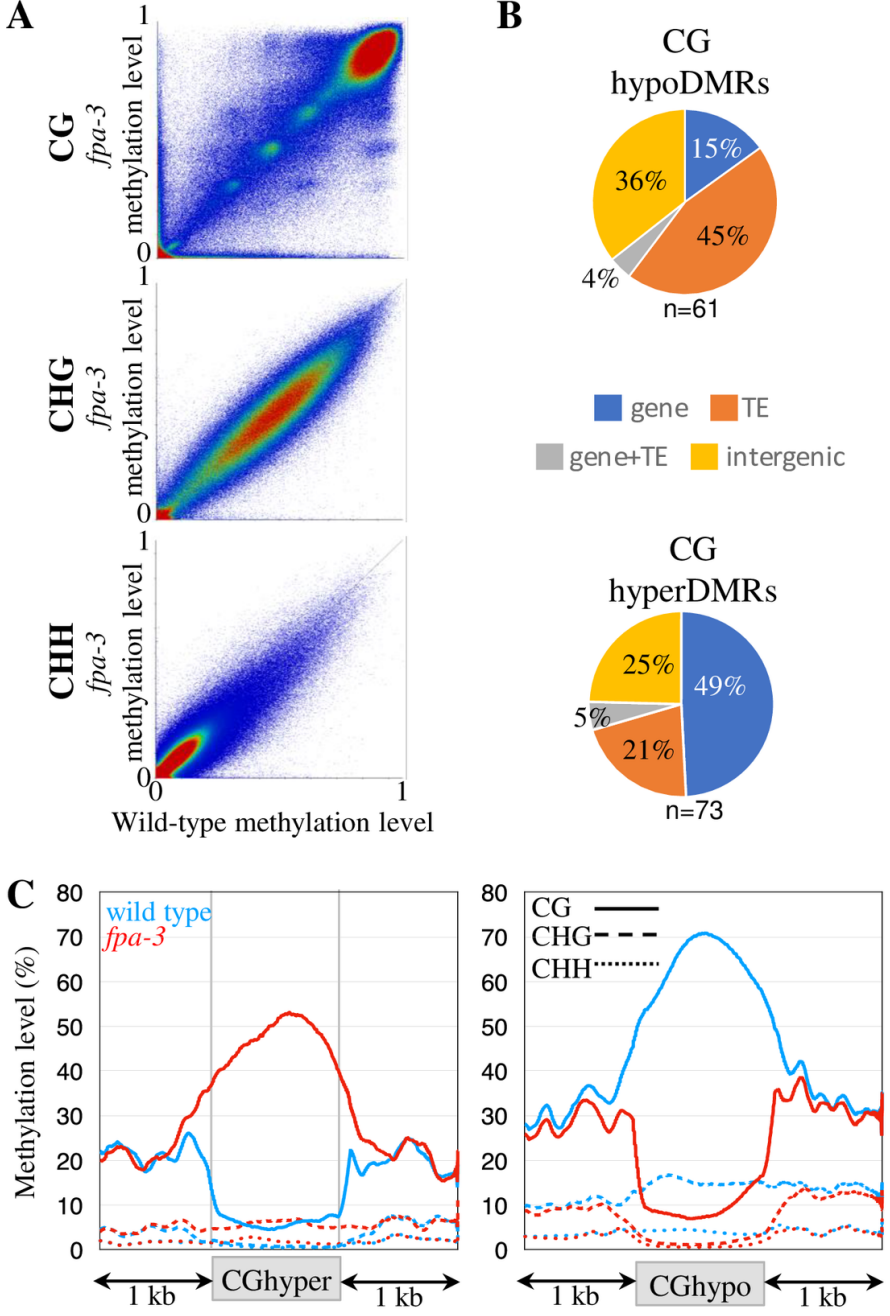

Figure 8. Patterns of methylation in *fpa*

(A) Pairwise comparison of methylation in wild type and *fpa-3* mutants. Each dot represents a 100 bp-window, and their methylation levels were determined as follows. The Arabidopsis genome (TAIR10 release) was partitioned in 100 bp-tiles and methylation levels correspond to the ratios of methylated cytosines over the total number of cytosines. Only cytosines covered by at least five reads were considered. The average methylation levels were determined by combining the two biological replicates for each genotype. The color scale measures the density of points (red being very dense). The Pearson correlation coefficients between the samples are 0.97 for mCG, 0.98 for mCHG and 0.94 for mCHH.

(B) Nature of CG hypo- and hyperDMRs identified in *fpa-3*. '*gene+TE*' corresponds to DMRs overlapping with both genes and transposons, '*gene*' corresponds to DMRs overlapping with genes, and '*TE*' corresponds to DMRs overlapping with transposons. All other DMRs were classified as '*Intergenic*'.

(C) Methylation levels of CG hypo- and hyperDMRs. The average methylation levels of the DMRs were determined by dividing the DMR into 100 bp bins. Regions located 1 kb upstream and 1 kb downstream are shown.

Parsed Citations

Bäurle I, Smith L, Baulcombe DC, Dean C (2007) Widespread role for the flowering-time regulators FCA and FPA in RNA-mediated chromatin silencing. Science 318: 109-112

Pubmed: Author and Title
Google Scholar: Author Only Title Only Author and Title

Corem S, Doron-Faigenboim A, Jouffroy O, Maumus F, Arazi T, Bouché N (2018) Redistribution of CHH methylation and small interfering RNAs across the genome of tomato ddm1 mutants. Plant Cell 7:1628-1644

Pubmed: Author and Title
Google Scholar: Author Only Title Only Author and Title

Coustham V, Vlad D, Deremetz A, Gy I, Cubillos FA, Kerdaffrec E, Loudet O, Bouché N (2014) SHOOT GROWTH1 maintains Arabidopsis epigenomes by regulating IBM1. PLoS One 9: e84687

Pubmed: Author and Title
Google Scholar: Author Only Title Only Author and Title

Du J, Johnson LM, Groth M, Feng S, Hale CJ, Li S, Vashisht AA, Gallego-Bartolome J, Wohlschlegel JA, Patel DJ, Jacobsen SE (2014) Mechanism of DNA methylation-directed histone methylation by KRYPTONITE. Mol Cell 55: 495-504

Pubmed: Author and Title
Google Scholar: Author Only Title Only Author and Title

Du J, Zhong X, Bernatavichute YV, Stroud H, Feng S, Caro E, Vashisht AA, Terragni J, Chin HG, Tu A, Hetzel J, Wohlschlegel JA, Pradhan S, Patel DJ, Jacobsen SE (2012) Dual binding of chromomethylase domains to H3K9me2-containing nucleosomes directs DNA methylation in plants. Cell 151: 167-180

Pubmed: Author and Title
Google Scholar: Author Only Title Only Author and Title

Duan CG, Wang X, Zhang L, Xiong X, Zhang Z, Tang K, Pan L, Hsu CC, Xu H, Tao WA, Zhang H, Zhu JK (2017) A protein complex regulates RNA processing of intronic heterochromatin-containing genes in Arabidopsis. Proc Natl Acad Sci U S A 114: E7377-e7384

Pubmed: Author and Title
Google Scholar: Author Only Title Only Author and Title

Duc C, Sherstnev A, Cole C, Barton GJ, Simpson GG (2013) Transcription termination and chimeric RNA formation controlled by Arabidopsis thaliana FPA. PLoS Genet 9: e1003867

Pubmed: Author and Title
Google Scholar: Author Only Title Only Author and Title

Ebbs ML, Bender J (2006) Locus-specific control of DNA methylation by the Arabidopsis SUVH5 histone methyltransferase. Plant Cell 18: 1166-1176

Pubmed: Author and Title
Google Scholar: Author Only Title Only Author and Title

Eulgem T, Tsuchiya T, Wang XJ, Beasley B, Cuzick A, Tor M, Zhu T, McDowell JM, Holub E, Dangl JL (2007) EDM2 is required for RPP7-dependent disease resistance in Arabidopsis and affects RPP7 transcript levels. Plant J 49: 829-839

Pubmed: Author and Title
Google Scholar: Author Only Title Only Author and Title

Fan D, Dai Y, Wang X, Wang Z, He H, Yang H, Cao Y, Deng XW, Ma L (2012) IBM1, a JmjC domain-containing histone demethylase, is involved in the regulation of RNA-directed DNA methylation through the epigenetic control of RDR2 and DCL3 expression in Arabidopsis. Nucleic Acids Res 40: 8905-8916

Pubmed: Author and Title
Google Scholar: Author Only Title Only Author and Title

García AV, Blanvillain-Baufumé S, Huibers RP, Wiermer M, Li G, Gobbato E, Rietz S, Parker JE (2010) Balanced Nuclear and Cytoplasmic Activities of EDS1 Are Required for a Complete Plant Innate Immune Response. PLoS Pathog 6

Pubmed: Author and Title
Google Scholar: Author Only Title Only Author and Title

Girard C, Crismani W, Froger N, Mazel J, Lemhemdi A, Horlow C, Mercier R (2014) FANCM-associated proteins MHF1 and MHF2, but not the other Fanconi anemia factors, limit meiotic crossovers. Nucleic Acids Res 42: 9087-9095

Pubmed: Author and Title
Google Scholar: Author Only Title Only Author and Title

Gruntman E, Qi Y, Slotkin RK, Roeder T, Martienssen RA, Sachidanandam R (2008) Kismeth: Analyzer of plant methylation states through bisulfite sequencing. In BMC Bioinformatics, Vol 9. BioMed Central Ltd, p 371

Pubmed: Author and Title
Google Scholar: Author Only Title Only Author and Title

Hansen KD, Langmead B, Irizarry RA (2012) BSmooth: from whole genome bisulfite sequencing reads to differentially methylated regions. Genome Biol 13: R83

Pubmed: Author and Title
Google Scholar: Author Only Title Only Author and Title

Hornyik C, Duc C, Rataj K, Terzi LC, Simpson GG (2010) Alternative polyadenylation of antisense RNAs and flowering time control. Biochem Soc Trans 38: 1077-1081
Pubmed: Author and Title
Google Scholar: Author Only Title Only Author and Title

Hornyik C, Terzi LC, Simpson GG (2010) The spen family protein FPA controls alternative cleavage and polyadenylation of RNA. Dev Cell 18: 203-213
Pubmed: Author and Title
Google Scholar: Author Only Title Only Author and Title

Inagaki S, Miura-Kamio A, Nakamura Y, Lu F, Cui X, Cao X, Kimura H, Saze H, Kakutani T (2010) Autocatalytic differentiation of epigenetic modifications within the Arabidopsis genome. EMBO J 29: 3496-3506
Pubmed: Author and Title
Google Scholar: Author Only Title Only Author and Title

Johnson LM, Bostick M, Zhang X, Kraft E, Henderson I, Callis J, Jacobsen SE (2007) The SRA methyl-cytosine-binding domain links DNA and histone methylation. Curr Biol 17: 379-384
Pubmed: Author and Title
Google Scholar: Author Only Title Only Author and Title

Kim D, Langmead B, Salzberg SL (2015) HISAT: a fast spliced aligner with low memory requirements. Nature Methods 12: 357
Pubmed: Author and Title
Google Scholar: Author Only Title Only Author and Title

Kim D, Pertea G, Trapnell C, Pimentel H, Kelley R, Salzberg SL (2013) TopHat2: accurate alignment of transcriptomes in the presence of insertions, deletions and gene fusions. Genome Biol 14: R36
Pubmed: Author and Title
Google Scholar: Author Only Title Only Author and Title

Koch E, Slusarenko A (1990) Arabidopsis is susceptible to infection by a downy mildew fungus. Plant Cell 2: 437-445
Pubmed: Author and Title
Google Scholar: Author Only Title Only Author and Title

Lai Y, Cuzick A, Lu XM, Wang J, Katiyar N, Tsuchiya T, Le Roch K, McDowell JM, Holub E, Eulgem T (2018) The Arabidopsis RRM domain protein EDM3 mediates race-specific disease resistance by controlling H3K9me2-dependent alternative polyadenylation of RPP7 immune receptor transcripts. Plant J doi:10.1111/tpj.14148
Pubmed: Author and Title
Google Scholar: Author Only Title Only Author and Title

Le TN, Miyazaki Y, Takuno S, Saze H (2015) Epigenetic regulation of intragenic transposable elements impacts gene transcription in Arabidopsis thaliana. Nucleic Acids Res 43: 3911-3921
Pubmed: Author and Title
Google Scholar: Author Only Title Only Author and Title

Liu F, Marquardt S, Lister C, Swiezewski S, Dean C (2010) Targeted 3' processing of antisense transcripts triggers Arabidopsis FLC chromatin silencing. Science 327: 94-97
Pubmed: Author and Title
Google Scholar: Author Only Title Only Author and Title

Love MI, Huber W, Anders S (2014) Moderated estimation of fold change and dispersion for RNA-seq data with DESeq2. Genome Biol 15: 550
Pubmed: Author and Title
Google Scholar: Author Only Title Only Author and Title

Lyons R, Iwase A, Gansewig T, Sherstnev A, Duc C, Barton GJ, Hanada K, Higuchi-Takeuchi M, Matsui M, Sugimoto K, Kazan K, Simpson GG, Shirasu K (2013) The RNA-binding protein FPA regulates flg22-triggered defense responses and transcription factor activity by alternative polyadenylation. Sci Rep 3: 2866
Pubmed: Author and Title
Google Scholar: Author Only Title Only Author and Title

Macknight R, Duroux M, Laurie R, Dijkwel P, Simpson G, Dean C (2002) Functional significance of the alternative transcript processing of the Arabidopsis floral promoter FCA. Plant Cell 14: 877-888
Pubmed: Author and Title
Google Scholar: Author Only Title Only Author and Title

Michaels SD, Amasino RM (2001) Loss of FLOWERING LOCUS C activity eliminates the late-flowering phenotype of FRIGIDA and autonomous pathway mutations but not responsiveness to vernalization. Plant Cell 13: 935-941
Pubmed: Author and Title
Google Scholar: Author Only Title Only Author and Title

Miura A, Nakamura M, Inagaki S, Kobayashi A, Saze H, Kakutani T (2009) An Arabidopsis jmjC domain protein protects transcribed genes from DNA methylation at CHG sites. EMBO J 28: 1078-1086
Pubmed: Author and Title
Google Scholar: Author Only Title Only Author and Title

Ong-Abdullah M, Ordway JM, Jiang N, Ooi SE, Kok SY, Sarpan N, Azimi N, Hashim AT, Ishak Z, Rosli SK, Malike FA, Bakar NA, Marjuni M, Abdullah N, Yaakub Z, Amiruddin MD, Nookiah R, Singh R, Low ET, Chan KL, Azizi N, Smith SW, Bacher B, Budiman MA, Van Brunt A, Wischmeyer C, Beil M, Hogan M, Lakey N, Lim CC, Arulandoo X, Wong CK, Choo CN, Wong WC, Kwan YY, Alwee SS, Sambanthamurthi R, Martienssen RA (2015) Loss of Karma transposon methylation underlies the mantled somaclonal variant of oil palm. Nature 525: 533-537

Pubmed: Author and Title
Google Scholar: Author Only Title Only Author and Title

Patil DP, Chen CK, Pickering BF, Chow A, Jackson C, Guttman M, Jaffrey SR (2016) m6A RNA methylation promotes XIST-mediated transcriptional repression. Nature 537: 369-373

Pubmed: Author and Title
Google Scholar: Author Only Title Only Author and Title

Ramírez F, Ryan DP, Grüning B, Bhardwaj V, Kilpert F, Richter AS, Heyne S, Dündar F, Manke T (2018) deepTools2: a next generation web server for deep-sequencing data analysis. Nucleic Acids Research 44: W160-5.

Pubmed: Author and Title
Google Scholar: Author Only Title Only Author and Title

Rigal M, Kevei Z, Pelissier T, Mathieu O (2012) DNA methylation in an intron of the IBM1 histone demethylase gene stabilizes chromatin modification patterns. EMBO J 31: 2981-2993

Pubmed: Author and Title
Google Scholar: Author Only Title Only Author and Title

Saze H, Kitayama J, Takashima K, Miura S, Harukawa Y, Ito T, Kakutani T (2013) Mechanism for full-length RNA processing of Arabidopsis genes containing intragenic heterochromatin. Nat Commun 4: 2301

Pubmed: Author and Title
Google Scholar: Author Only Title Only Author and Title

Saze H, Shiraishi A, Miura A, Kakutani T (2008) Control of genic DNA methylation by a jmjC domain-containing protein in Arabidopsis thaliana. Science 319: 462-465

Pubmed: Author and Title
Google Scholar: Author Only Title Only Author and Title

Slusarenko AJ, Schlaich NL (2003) Downy mildew of Arabidopsis thaliana caused by Hyaloperonospora parasitica (formerly Peronospora parasitica). Mol Plant Pathol 4: 159-170

Pubmed: Author and Title
Google Scholar: Author Only Title Only Author and Title

Sonmez C, Bäurle I, Magusin A, Dreos R, Laubinger S, Weigel D, Dean C (2011) RNA 3' processing functions of Arabidopsis FCA and FPA limit intergenic transcription. Proc Natl Acad Sci U S A 108: 8508-8513

Pubmed: Author and Title
Google Scholar: Author Only Title Only Author and Title

Stroud H, Greenberg MV, Feng S, Bernatavichute YV, Jacobsen SE (2013) Comprehensive analysis of silencing mutants reveals complex regulation of the Arabidopsis methylome. Cell 152: 352-364

Pubmed: Author and Title
Google Scholar: Author Only Title Only Author and Title

Stroud H, Hale CJ, Feng S, Caro E, Jacob Y, Michaels SD, Jacobsen SE (2012) DNA methyltransferases are required to induce heterochromatic re-replication in Arabidopsis. PLoS Genet 8: e1002808

Pubmed: Author and Title
Google Scholar: Author Only Title Only Author and Title

Sun YW, Tee CS, Ma YH, Wang G, Yao XM, Ye J (2015) Attenuation of Histone Methyltransferase KRYPTONITE-mediated transcriptional gene silencing by Geminivirus. Sci Rep 5: 16476

Pubmed: Author and Title
Google Scholar: Author Only Title Only Author and Title

Tsuchiya T, Eulgem T (2013) An alternative polyadenylation mechanism coopted to the Arabidopsis RPP7 gene through intronic retrotransposon domestication. Proc Natl Acad Sci U S A 110: E3535-3543

Pubmed: Author and Title
Google Scholar: Author Only Title Only Author and Title

Tsuchiya T, Eulgem T (2013) Mutations in EDM2 selectively affect silencing states of transposons and induce plant developmental plasticity. Sci Rep 3: 1701

Pubmed: Author and Title
Google Scholar: Author Only Title Only Author and Title

Veley KM, Michaels SD (2008) Functional redundancy and new roles for genes of the autonomous floral-promotion pathway. Plant Physiol 147: 682-695

Pubmed: Author and Title
Google Scholar: Author Only Title Only Author and Title

Wang X, Duan CG, Tang K, Wang B, Zhang H, Lei M, Lu K, Mangrauthia SK, Wang P, Zhu G, Zhao Y, Zhu JK (2013) RNA-binding protein

regulates plant DNA methylation by controlling mRNA processing at the intronic heterochromatin-containing gene IBM1. Proc Natl Acad Sci U S A 110: 15467-15472
Pubmed: Author and Title
Google Scholar: Author Only Title Only Author and Title

Wang YH, Warren JT, Jr. (2010) Mutations in retrotransposon AtCOPIA4 compromises resistance to Hyaloperonospora parasitica in Arabidopsis thaliana. Genet Mol Biol 33: 135-140
Pubmed: Author and Title
Google Scholar: Author Only Title Only Author and Title

Wu H, Xu T, Feng H, Chen L, Li B, Yao B, Qin Z, Jin P, Conneely KN (2015) Detection of differentially methylated regions from whole-genome bisulfite sequencing data without replicates. Nucleic Acids Res 43:e141.
Pubmed: Author and Title
Google Scholar: Author Only Title Only Author and Title

Wu Z, Ietswaart R, Liu F, Yang H, Howard M, Dean C (2016) Quantitative regulation of FLC via coordinated transcriptional initiation and elongation. Proc Natl Acad Sci U S A 113: 218-223
Pubmed: Author and Title
Google Scholar: Author Only Title Only Author and Title

Zhang Y, Harris CJ, Liu Q, Liu W, Ausin I, Long Y, Xiao L, Feng L, Chen X, Xie Y, Zhan L, Feng S, Li JJ, Wang H, Zhai J, Jacobsen SE (2018) Large-scale comparative epigenomics reveals hierarchical regulation of non-CG methylation in Arabidopsis. In Proc Natl Acad Sci U S A, 115: 1069-1074
Pubmed: Author and Title
Google Scholar: Author Only Title Only Author and Title

Zhang Y, Li X, Goodrich J, Wu C, Wei H, Yang S, Feng X (2016) Reduced function of the RNA-binding protein FPA rescues a T-DNA insertion mutant in the Arabidopsis ZHOUPI gene by promoting transcriptional read-through. Plant Mol Biol 91: 549-561
Pubmed: Author and Title
Google Scholar: Author Only Title Only Author and Title